BUREAU OF RECLAMATION

Assessing Reservoir Sedimentation Using Multidate Landsat Imagery

Research and Development Office
Science and Technology Program
Final Report ENV-2020-014

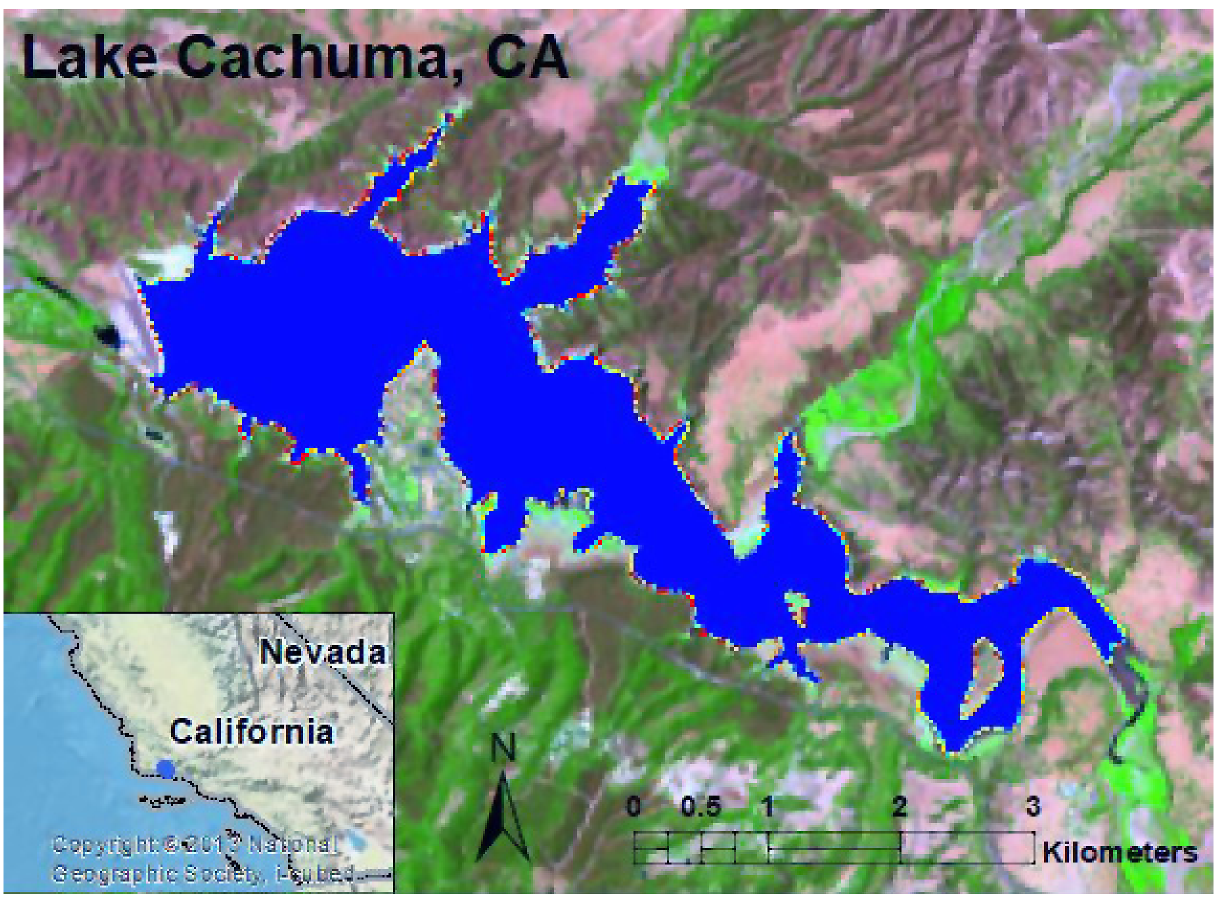

U.S. Department of the Interior
Bureau of Reclamation
Research and Development Office

December 2019

Mission Statements

The Department of the Interior (DOI) conserves and manages the Nation's natural resources and cultural heritage for the benefit and enjoyment of the American people, provides scientific and other information about natural resources and natural hazards to address societal challenges and create opportunities for the American people, and honors the Nation's trust responsibilities or special commitments to American Indians, Alaska Natives, and affiliated island communities to help them prosper.

The mission of the Bureau of Reclamation is to manage, develop, and protect water and related resources in an environmentally and economically sound manner in the interest of the American public.

Cover: image of a color-coded map of water proportions from which reservoir surface area is calculated.

REPORT DOCUMENTATION PAGE

Form Approved
OMB No. 0704-0188

T1. REPORT DATE:
DECEMBER 2019

T2. REPORT TYPE:
RESEARCH

T3. DATES COVERED

T4. TITLE AND SUBTITLE
Assessing Reservoir Sedimentation Using Multidate Landsat Imagery

5a. CONTRACT NUMBER

5b. GRANT NUMBER

5c. PROGRAM ELEMENT NUMBER
1541 (S&T)

6. AUTHOR(S)
Dave Eckhardt, Physical Scientist
Geographic Applications & Analysis
DEckhardt@usbr.gov

5d. PROJECT NUMBER
Prize Comp: Indirect Water Storage Estimates Next Steps

5e. TASK NUMBER

5f. WORK UNIT NUMBER

7. PERFORMING ORGANIZATION NAME(S) AND ADDRESS(ES)

8. PERFORMING ORGANIZATION REPORT NUMBER
ENV-2020-014

9. SPONSORING / MONITORING AGENCY NAME(S) AND ADDRESS(ES)
Research and Development Office
U.S. Department of the Interior, Bureau of Reclamation,
PO Box 25007, Denver CO 80225-0007

10. SPONSOR/MONITOR'S ACRONYM(S)
R&D: Research and Development Office
BOR/USBR: Bureau of Reclamation
DOI: Department of the Interior

11. SPONSOR/MONITOR'S REPORT NUMBER(S)

12. DISTRIBUTION / AVAILABILITY STATEMENT
Final report can be downloaded from Reclamation's website: https://www.usbr.gov/research/

13. SUPPLEMENTARY NOTES

14. ABSTRACT ***(Maximum 200 words) This report describes a method of measuring reservoir surface area (RSA) using satellite imagery and demonstrates that a time series of these measurements made at differing reservoir elevations can be used to measure reservoir storage capacity within the reservoir elevation range observed in the imagery. Similar measurements over time can be used to estimate the rate of reservoir sedimentation.***

15. SUBJECT TERMS reservoir, satellite, surface area

16. SECURITY CLASSIFICATION OF:			**17. LIMITATION OF ABSTRACT**	**18. NUMBER OF PAGES**	**19a. NAME OF RESPONSIBLE PERSON**
a. REPORT U	**b. ABSTRACT** U	**c. THIS PAGE** U	U		**19b. TELEPHONE NUMBER**

S Standard Form 298 (Rev. 8/98)
P Prescribed by ANSI Std. 239-18

BUREAU OF RECLAMATION
Technical Service Center, Denver, Colorado
Geographic Applications & Analysis Group, 86-68260

Research and Development Office
Science and Technology Program
Final Report ENV-2020-014

Assessing Reservoir Sedimentation Using Multidate Landsat Imagery

David Eckhardt

Prepared: David Eckhardt, Physical Scientist, Geographic Applications and Analysis Group, 86-68260

Stephen D Belew

Peer Review: Stephen Belew, Hydraulic Engineer (GIS), Geographic Applications and Analysis Group, 86-68260

Timothy J. Randle

Peer Review: Timothy Randle, Manager, Sedimentation and River Hydraylics Group, 86-68240

Assessing Reservoir Sedimentation Using Multidate Landsat Imagery

Abstract

This report describes a method of measuring reservoir surface area (RSA) using satellite imagery, and demonstrates that a time series of these measurements made at differing reservoir elevations can be used to measure reservoir storage capacity within the reservoir elevation range observed in the imagery. Similar measurements over time can be used to estimate the rate of reservoir sedimentation.

125 Landsat satellite images of six Bureau of Reclamation reservoirs (Bighorn Reservoir MT/WY, Black Canyon Reservoir ID, Elephant Butte Reservoir NM, Lake Cachuma CA, Lake Mead AZ/NV, and Paonia Reservoir CO) were processed to illustrate these capabilities. Thresholding the first shortwave infrared spectral band (SWIR1) of Landsat images identifies pixels containing 100% water, and subsequent processing identifies shoreline and land pixels adjacent to the water pixels. Water proportion in each shoreline pixel is estimated using a linear mixture model that compares the SWIR1 reflectance of the shoreline pixels to that from adjacent land and water pixels. Proportions of each water and shoreline pixel within a given image are summed, and the sum multiplied by the area of each Landsat pixel (900 m^2) to estimate RSA.

Reservoir volume between any two observed reservoir elevations is estimated using a formula that assumes constant terrain slope between the two reservoir elevations. Reservoir volume over a large elevation ranges characterized by multiple images is calculated as the sum of all the volume 'slices' of the reservoir represented by the image data. Reservoir volumes measured at different points in time can be used to estimate reservoir sedimentation rates.

Although images used to map RSA at multiple reservoir elevations were acquired over date ranges from 4 to 15 years, reservoir surface area and volume estimates generated from the Landsat imagery compare favorably to area and volume estimates generated from conventional reservoir bathymetric survey data. Summed Landsat-derived reservoir surface area estimates for all reservoirs are 0.9% less than the summed estimates from the surveys performed closest in time to the Landsat image acquisitions for a particular reservoir. If the comparison is limited to data from imagery acquired within one year of the reservoir survey, the difference is reduced to 0.5%. For individual reservoirs, Elephant Butte Reservoir, whose image acquisition dates most closely matched the survey date, had the closest match between Landsat-derived and surveyed values, with Landsat-derived surface area and volume estimates being 0.2% less than survey-based estimates. The greatest discrepancies for an individual reservoir were seen for Bighorn Reservoir, where Landsat-derived surface area and volume estimates were 2.1% and 2.4% less than survey-derived values, respectively.

Assessing reservoir surface area and volumes using satellite imagery is an inexpensive way to provide a first-order estimate of reservoir sedimentation, either using a time series of images acquired at the same reservoir elevation to observe reductions in surface area over time, or using image sets that capture large reservoir elevation ranges from which reservoir volume estimates can be derived. However, this method cannot be considered a substitute for

conventional reservoir surveys because sedimentation cannot be measured below the lowest reservoir elevation represented in an image set, and because measurements are inextricably linked to the time series of reservoir elevations and the availability of cloud-free imagery, which may or may not be suitable for making the desired measurements. And due to the inevitable addition and redistribution of sediment within a reservoir during the time period of reservoir drawdown or filling needed for to calculate reservoir volume using this method, measurements will always differ slightly from conventional surveys which usually take place over a much shorter time period.

Introduction

In the absence of sediment management, all reservoirs have a finite lifetime, as sedimentation gradually reduces available storage volume over time. These reductions are quantified using hydrographic surveys that measure changes to reservoir bathymetry over time. Bathymetric survey data obtained from singlebeam or multibeam echo sounder data at a given reservoir elevation are combined with terrestrial elevation data generated from either high-resolution image or LiDAR (light detection and ranging) data acquired when the reservoir is at a lower elevation. The result is a continuous bathymetric surface from maximum pool elevation to the bottom of the reservoir, from which reservoir surface areas and volumes can be calculated.

Ideally, bathymetric reservoir surveys are conducted about once per decade and typically cost between \$50,000 to \$500,000, require one or two weeks of field data collection, and a few months of staff time to process the data and produce new and detailed surface area and storage capacity tables. In between these detailed bathymetric surveys, a less expensive and coarser method is to use satellite measurements of RSA to assess reduced reservoir surface area and volumes due to sedimentation. Although numerous earth resource satellites provide imagery that could be used for this application, Landsat images were chosen for use in this study because the Landsat archive contains radiometrically-calibrated and orthorectified moderate-resolution imagery (30 m pixel size) going back to 1984, all of which are available free of charge from the U.S. Geological Survey. The consistent nadir-look of the Landsat satellites also limits sun glint from lakes and reservoirs, allowing for more reliable, automated identification of water pixels.

Reservoir volume between any two observed reservoir surface elevations was estimated using a equation for the volume of a pyramidal frustum, as presented in Abileah et al., 2011:

$$\Delta V = ((H_1 - H_0) * (A_1 + A_0 + \mathrm{sqrt}(A_1 * A_0))) / 3 \qquad \text{Equation 1}$$

where:

ΔV	=	volume between two measured elevations and areas
H_1, H_0	=	reservoir elevations at dates T_1 and T_0, respectively
A_1, A_0	=	reservoir surface area at dates T_1 and T_0, respectively

This formula assumes constant terrain slopes between successive RSA measurements made at differing reservoir elevations, which is reasonable in most cases. Reservoir volume is calculated as the sum of all ‘slices’ of the reservoir represented by the image data. It is important to note that the remote sensing method cannot measure sedimentation below the lowest observed reservoir elevation.

Reclamation compared the elevation tables for six Reclamation reservoirs to the acquisition dates of cloud-free Landsat imagery, and selected 115 images for processing that documented a wide range of water surface elevations at each reservoir. These data were used to develop hypsometry curves for each reservoir that are associated with the date range of image acquisitions. The reservoirs whose surface areas were mapped using remote sensing are listed in Table 1, along with the states and Reclamation Regions in which they are located, the number of Landsat images that were processed, and the date range of those images.

Table 1. Date Range of Landstat Images

Reservoir	State	BOR Region	No. Landsat Images	Date Range
Bighorn Lake	MT/WY	Great Plains	18	2003 –2018
Black Canyon Reservoir	ID	Pacific Northwest	5	2002
Elephant Butte Reservoir	NM	Upper Colorado	21	1998 – 2002
Lake Cachuma	CA	Mid Pacific	22	2011 – 2016
Lake Mead	AZ/NV	Lower Colorado	30	2000 – 2016
Paonia Reservoir	CO	Upper Colorado	19	2010 – 2018

Reclamation processed an additional 10 Landsat images to document the reduction of surface area over time at three different water surface elevations at Elephant Butte Reservoir, New Mexico.

Background

A combination of a water body's height and water surface area at different dates can be used to establish a relationship between those variables and water volume. Because water bodies usually appear as spectrally distinct dark objects on optical satellite images, remote sensing is used as an efficient way to identify water bodies and provide the water surface area data required for volumetric calculations (Roman et al., 2010; Gao et al., 2012; Duan and Bastiaanssen, 2013; Arsen et al., 2014). Water bodies usually appear as spectrally distinct dark objects on satellite images because water is a strong absorber of solar radiation, particularly in near infrared through shortwave infrared wavelengths (0.8 – 2.5 μm). However, the spectral radiance of a water pixel measured at the spaceborne sensor is also affected by atmospheric scattering and absorption, scattering of skylight and direct sunlight off the water surface (i.e., 'sun glint'), and water volume reflectance – light reflected by the water column, primarily in response to dissolved substances and suspended particles, both organic and inorganic. Although images can be processed to largely remove atmospheric effects, reflectance variation arising from variation in sun glint and water volume reflectance remain. In addition, variation in spectral band placement and sensor response functions between different sensors also adds to the variability in spectral response seen from 'pure water' pixels.

Numerous spectral bands and band ratios have been developed in an attempt to reduce the impact of the factors listed above and to spectrally isolate water pixels from all non-water pixels – a task that is more difficult than one might expect given the wide variation of reflectance in both aquatic and terrestrial targets. Some of the spectral features used to discriminate water from land pixels include:

- ρ_{NIR} (near infrared reflectance)
- ρ_{SWIR1} (shortwave infrared reflectance centered near 1.62 μm)
- ρ_{SWIR2} (shortwave infrared reflectance centered near 2.21 μm)
- ρ_{red}, but only when $\rho_{NIR} < \rho_{red}$
- ρ_{green}/ρ_{NIR}
- NDVI (Normalized Difference Vegetation Index): $(\rho_{NIR} - \rho_{red}) / (\rho_{NIR} + \rho_{red})$
- NDWI (Normalized Difference Water Index): $(\rho_{green} - \rho_{NIR}) / (\rho_{green} + \rho_{NIR})$ (McFeeters, 1996)
- MNDWI (Modified NDWI): $(\rho_{green} - \rho_{SWIR1}) / (\rho_{green} + \rho_{SWIR1})$ (Xu, 2006)

Spectral features can be used in a number of ways to map water pixels, including simple thresholding (e.g., water if $\rho_{SWIR} < 0.06$) , analyst-defined decision tree logic (e.g., water if $\rho_{NIR} < \rho_{red} < \rho_{greem}$), supervised or non-supervised image classification, and machine learning approaches. However, due to the spectral variability of water pixels described above, spectral features and/or classifier logic may need to be modified when they are applied across time and/or space (Liu et al., 2012). If necessary, spatial filtering such as a 3x3 majority filter can be applied to the classifier output to eliminate isolated misclassifications (Gao et al., 2012).

For large lakes and reservoirs lacking the instrumentation needed to measure water surface elevation, satellite altimetry can provide that important information. The accuracy of water surface elevation measurements from satellite altimeters is quite good for large water bodies the size of the Great Lakes or larger, but drops off significantly to the multiple decimeter to meter level as water body size decreases. Comparisons of altimetry products with in situ daily gauge data show that the RMS accuracy ranges from a minimum of 3 cm for Lake Issyk-Kul, Kyrgyzstan (an ice-free lake greater than 1,500,000 acres in size), to a maximum of 80 cm for the smaller, narrower Lake Powell (~150,000 acres) (Ricko et al., 2012). For this project, reservoir volume estimates were generated from daily reservoir elevations measured at the dam and RSA estimates obtained from Landsat satellite imagery.

Reservoir Surface Area and Volume Estimation Procedures

Estimates from Landsat Imagery

RSA is computed by summing the individual areas of all pixels that are determined to be 100% water, and the water proportions of the pixels along the reservoir shoreline. 100% water pixels and the first of two 'rings' of shoreline pixels are identified using an image thresholding procedure. The second 'ring' of shoreline pixels are identified using spatial filtering that expands the initially-identified water and shoreline pixels outward by 1 pixel in all directions.

Numerous spectral bands and indices were investigated for use as a land/water discriminant, but none performed better than the Landsat SWIR1 spectral band. The extremely low reflectance of water in this band (typically < 2.0%) and its extremely shallow penetration depth (millimeters) combines with the generally high reflectance of bare soil (~30% to 40%) and moderate reflectance of vegetation (~10% to 20%) to provide good land/water contrast in most circumstances.

While typical SWIR1 reflectance of a calm, flat water surface is extremely low (from < 0.5% to 2%, depending on sun angle), reflectance values can increase substantially as a result of sun glint – the reflectance of direct beam (and to a much lesser extent, diffuse) solar radiation off the air/water interface into the imaging sensor. The severity of sun glint generally increases as sun elevations and/or water surface roughness increase. The lowest SWIR1 reflectance threshold capable of identifying the vast majority of water pixels on all images of a particular reservoir was applied to every image of that reservoir. And because increasing the SWIR1 reflectance threshold results in an increased number of 'water pixels' being identified in the initial image thresholding step (described below), a constant SWIR1 reflectance threshold of 6% was used for four of the six reservoirs where sun glint seen on the Landsat images was never extreme. This threshold had to be increased to 10% and 12% for Elephant Butte Reservoir and Lake Mead, respectively, because extreme sun glint was present on some of the late spring and early summer Landsat images.

Applying the elevated SWIR1 reflectance thresholds required to identify water pixels experiencing sun glint meant that pixels experiencing limited or no sun glint could contain a significant proportion of land (~25% or less) and still be identified as water. Consequently, a the outer ring of 'water' pixels around the perimeter of each reservoir nearly always contained a mixture of water and land. The pixels immediately upslope from those initial 'shoreline' pixels also contained a mixture of land and water, and were identified as shoreline as well. The two-pixel-wide ring upslope from the shorline pixels were identified as 'land' pixels and were assumed to contain no water. The water proportion assigned to all 'water' pixels was of course 1.0, and the water proportion assigned to all 'land' pixels was zero. The water proportion assigned to the shoreline pixels was estimated using a linear mixture model applied to each identified shoreline pixel:

$$W_{SHORE} = (\rho_{SWIR1,LAND} - \rho_{SWIR1,SHORE}) / (\rho_{SWIR1,LAND} - \rho_{SWIR1,WATER}) \quad \text{Equation 2}$$

where:

W_{SHORE} = proportion of water within a shoreline pixel
$\rho_{SWIR1,LAND}$ = Landsat SWIR1 reflectance of land pixels adjacent to the shoreline pixel
$\rho_{SWIR1,SHORE}$ = Landsat SWIR1 reflectance of the shoreline pixel
$\rho_{SWIR1,WATER}$ = Landsat SWIR1 reflectance of water pixels adjacent to the shoreline pixel

Both land and water reflectance values varied spatially around the perimeter of the reservoirs. Land values varied with the reflectance characteristics of the land cover as well as the local sun angle at the time of image acquisition; while water reflectance varied primarily with the severity of sun glint. To optimize water proportion estimates for the shoreline pixels, locally-measured land and water reflectance values were used in Equation 2. These values were obtained by first isolating the land and 100% water pixels and saving them as separate images. Then, a sequence of 3x3 moving average filters expanded mean land and water

SWIR1 reflectance values outward into the space occupied by the shoreline pixels, allowing Equation 2 to be executed using simple image arithmetic.

The following is the general procedure that was followed to generate reservoir surface area and volume estimates from multiple Landsat images for all six reservoirs. Additional processing steps were added to improve RSA estimates for two of the studied reservoirs. These are described in the site-specific descriptions in the next section of this report.

1) Acquire a database of daily reservoir elevations for the period of record that is in common with the years of operation of the spaceborne sensors being used.

2) Identify time periods during which the desired phenomenon can be measured (i.e., either a drawdown period to estimate a new reservoir volume between the low and high water marks, or a time series of views of the same reservoir water surface elevation).

3) View Landsat imagery using an online viewer and generate a list of cloud-free images during the desired time period.

4) From that list, order images that show the reservoir at elevation differences of approximately 5 feet. For this project, Reclamation ordered Landsat images processed to apparent surface reflectance using the USGS (United States Geological Survey) ESPA (EROS Science Processing Architecture) ordering interface (https://espa.cr.usgs.gov). ESPA allows for the reprojection of the Imagery into one of five output map projections. Images were left in their native UTM projection, with 30-meter pixels centered on integer multiples of 30 meters.

5) Acquire a 1 arc-second NED (National Elevation Dataset) DEM (digital elevaiton model) from the USGS of an area containing the reservoir. Reproject this DEM from its native geographic (lat/lon) map projection into the same projection and grid system as the Landsat images using cubic convolution resampling.

6) Define an AOI (area of interest) polygon for each satellite image that encompasses the reservoir to be processed. The polygon can be loosely drawn around most of the reservoir, but care must be taken to precisely identify the boundaries where tributaries flow into the reservoir. For this study, pools that occasionally occurred in the floodplain of the main tributary stream/river upstream of the reservoir were excluded from the RSA measurements, although they might have been hydraulically connected to the reservoir.

7) Carefully inspect the DEM to establish a maximum elevation threshold, above which no pixel can be identified as water. Shaded land pixels commonly have very low SWIR1 reflectance values that fall below the SWIR1 threshold used to identify water pixels, so an elevation threshold is a simple way to exclude those pixels from the water mask. DEMs are not consistent in their data quality, nor the stage of the reservoir that is depicted in the data. If high quality elevation data exist below the maximum reservoir elevation, decreasing elevation thresholds can be used as reservoir elevations fall. Even with the highest quality DEM, issues such as differences in the vertical datums used to measure elevations between reservoir records and the NED DEMs, breaks in slope on the DEM surface at the edge of the reservoir surface, and/or atrifacts produced by resampling the NED DEM necessitated the use of elevation thresholds that were a few meters higher than reported reservoir elevations.

8) Inspect each of the acquired satellite images, and note the minimum SWIR1 reflectance value that must be used to identify the vast majority of water pixels on all images. This value is used to map water pixels on all images of the reservoir.

9) Generate a temporary binary image mask by thresholding the SWIR1 images using the SWIR1 reflectance and DEM elevation thresholds described above. Identified pixels are coded as 1, and the rest are coded as 0. The SWIR1 reflectance threshold is set higher than that of a typical '100% water' pixel because it must identify water pixels experiencing significant sun glint, which increases water reflectance significantly. Consequently, nearly all of the identified pixels along the perimeter of the reservoir are not 100% water and contain some small percentage of land.

Output image: temp1

10) Exclude the outer ring of pixels identified in temp1 that contain a non-zero proportion of land by applying a 3x3 minimum filter to temp1. The result is a mask that identifies all 100% water pixels.

water_01mask

11) Expand temp1 from step 9 by one pixel in all directions using a 3x3 maximum filter. This identifies the second 'ring' of shoreline pixels that contain both water and land.

Output image: temp2

12) Generate a mask that identifies only shoreline pixels (the outermost pixels from temp1 and the shoreline pixels adjacent to them from temp2) by subtracting 'water_01mask' from 'temp2'

Output image: shore_01mask

13) Expand temp2 from step 11 by two pixels in all directions using a 5x5 maximum filter. This identifies the land pixels that will be used in the water proportion calculations.

Output image: temp3

14) Subtract the water and shoreline pixels in temp2 from temp3 to generate a mask of land pixels.

Output image: land_01mask

15) Mask the SWIR reflectance image with 'water_01mask' to create an image of 100% water pixels

Output image: water

16) Expand data values in the 'water' image outward by 9 pixels in all directions by running a series of nine 3x3 averaging operations. The averaging operation is only applied to background pixels (coded with zeros), and only uses valid (i.e., non-background) image data

in its calculations. Assign the mean SWIR reflectance value from the 'water' image to the remaining background pixels. This large expansion of the spatial coverage of water pixels is necessary because there are many small, narrow inlets on some of the reservoirs where the identified water areas are only a pixel or two wide. When the initial temp1 mask is reduced in size by one pixel in all directions to identify 'pure' water pixels, the narrow clumps of identified shoreline pixels in temp1 disappear. To provide all shoreline pixels with locally-measured local water reflectance for use in Equation 2, the 'water' image must be expanded significantly.

Output image: water_out9

17) Mask the SWIR reflectance image with 'land_01mask' to create an image of 100% land pixels.

Output image: land

18) Expand data values in the 'land' image outward by 4 pixels in all directions by running a series of four 3x3 averaging operations, where the operation is only applied at background pixel locations, and only uses valid (i.e., non-background) image data in its calculations. Assign the mean SWIR reflectance value from the 'land' image to all remaining background pixels.

Output image: land_out4

19) Mask the SWIR reflectance image with 'shore_01mask' to create a SWIR1 image containing only shoreline pixels.

Output image: shore

20) Calculate the proportion of water within the shoreline pixels in 'shore' using Equation 2, substituting 'land_out4', 'shore', and 'water_out9', for '$\varrho_{SWIR1,LAND}$', '$\varrho_{SWIR1,SHORE}$', and '$\varrho_{SWIR1,\ WATER}$', respectively. Clip calculated water proportions to fall within the 0.0001 to 1.0000 data range, then insert the 'water' image (which contain proportion values of 1.0 for every pixel). This generates the final water proportion image (Figure 1).

Output image: waterprop

21) If necessary, manually edit the 'waterprop' image to fix any obvious omission errors resulting from bridges, floating marinas, extreme sun glint, floating algae mats, or commission errors occurring in terrain shadows or nearby water bodies.

Output image: waterprop

22) Sum all of the image pixel values within 'waterprop', and multiply the result by the area of each image pixel (30 m x 30 m = 900 m^2 = 0.222394843 acres for the Landsat pixels used in this study) to generate the final reservoir surface area.

RSA values from both the remote sensing and reservoir survey analyses were not corrected for slight differences in surface area calculated from an image (remote sensing) or terrain model (reservoir survey) in a particular map projection, compared to on-the-ground surface area. Such differences arise from 'grid scale' factors that relate to areal distortions inherent to the map projection, and 'elevation scale' factors that relate to areal distortions related to the elevation of the measured feature above or below the reference Earth ellipsoid. Calculated grid scale and elevation scale factors for the centroid of each reservoir in this study indicate that the largest difference between remotely sensed and on-the-ground area was less than 0.01% for Lake Cachuma, which lies on the periphery of UTM zone 11. Consequently, grid scale and elevation scale errors were deemed insignificant for the purposes of this study.

Once all of the Landsat images for a particular reservoir had been processed, reservoir volume between successive reservoir elevations documented by the Landsat images was calculated using Equation 1. Reservoir volume between the maximum and minimum reservoir surface elevations was calculated as the sum of all of the volumetric 'slices' of the reservoir represented by the image data. Absolute calibration of elevations to a particular vertical datum is irrelevant for the purposes of reservoir volume estimation. In all cases, elevations recorded at each dam were relative to a local Reclamation datum, and these elevations were used in the volumetric calculations.

Estimates from Reservoir Survey Data

For all but Black Canyon Reservoir, conventioal reservoir surveys were conducted during the time period during which the Landsat images of each reservoir were acquired. Prior to the year 2000, most reservoir surveys were done using range lines, where crews in boats traversed reservoirs along previously surveyed transects, taking continual depth measurementsalong those lines. Combined with reservoir elevation data at the time the transect was traversed, bottom elevations were derived. The deepest depth measurement along each range line was assumed to be the 'new' bottom of the reservoir, and the bathymetric data from the previous survey (or the pre-dam topographic map if no previous surveys were done) were updated with the new measurements.

After 2000, the use of GPS instruments to continuosly measure the position of the survey boats started to be used. These instruments could be used to collect data at all locations in a reservoir. Depths could be sounded in water just a few feet deep to several hundred feet deep. GPS instruments allowed for a much more complete bathymetric dataset. When hydrographic surveys were done below full pool elevaiton of the reservoir, the bathymetric data were usually combined with older terrestrial data, often from the predam survey. In later years (after 2000), LiDAR became available to provide above-water data for some reservoir surveys and LiDAR is becomming more available with each passing year. The availability LiDAR-based elevation data or photogrammetric data provides a seamless bathymetric dataset for the entire reservoir. These data are then used to generate a terrain model in ArcGIS, and software was used to automatically generate surface areas for the reservoir at specified reservoir elevations, and to calculate reservoir volumes from the bottom of the reservoir to the defined reservoir elevations. For this project, tabular listings of reservoir surface areas and volumes by reservoir elevation were used in the analysis.

When comparing RSA data derived from Landsat imagery and reservoir survey data, RSA data derived from survey data were linearly interpolated on the basis of reservoir elevation to generate RSA values for the same reservoir elevations as depicted on the Landsat images. When comparing reservoir volumes, the reverse was done: RSA values derived from the Landsat imagery were linearly interpolated to exactly match the elevations listed in the survey report before calculating volumes using Equation 1. The only exception to this rule was for Black Canyon Reservoir, where an extrememly granular reservoir elevation/area/volume table (0.5-foot increments) was linearly interpolated to match the reservoir elevations seen in the Landsat imagery. Comparisons of reservoir surface area and volume estimates for all six reservoirs are presented in Table 2.

Table 2. Mean surface areas on Landsat image acquisition dates and volumes between the maximum and minimum reservoir elevations recorded by the Landsat imagery for the six reservoirs investigated in this study

Reservoir	Mean Landsat RSA (acres)	Mean Survey RSA (acres)	Landsat RSA / Survey RSA	Landsat Volume	Survey Volume	Landsat Volume/ Survey Volume
Bighorn	8775	8963	0.9790	640402	655990	0.9762
Black Canyon	412.9	415.7	0.9928	11793	12013	0.9817
Cachuma	1615	1633	0.9890	165961	167664	0.9898
Elephant Butte	17706	17741	0.9980	1657240	1661048	0.9977
Mead	103300	104295 (2001)	0.9905 (2001)	11474625	11580950 (2001)	0.9908 (2001)
Mead	103300	105509 (2009)	0.9791 (2009)	11474625	11717491 (2009)	0.9793 (2009)
Paonia	199.2	203.4	0.9794	15353	15579	0.9855

Reservoir surveys are not without error, and reservoir surface areas and volumes calculated from survey data should not be considered 'ground truth' (especially when predam survey data are used to represent the above-water reservoir topography). Information presented below will assist in the interpretation of the data presented in Table 2.

Site Specific Processing Procedures for Volumetric Analyses

Lake Cachuma, CA

Surface area at full pool:	3300 acres
Approximate full pool elevation:	753 ft
Max. SWIR1 reflectance threshold:	6%
Max. DEM elevation threshold:	755 – 791 ft (230 to 241 m), depending on lake elevation
Date range of image acquisitions:	April 2011 – October 2016
Closest in time reservoir survey:	December, 2013

Lake Cachuma is a storage reservoir on the Santa Ynez River, 18 miles northwest of Santa Barbara, California (Figure 2). The reservoir is formed by Bradbury Dam (completed in 1953), and is located in a semi-arid Mediterranean environment. Shoreline vegatation consists primarily of shrubs and grasses, with broadleaf forest and woodland on north-facing slopes.

RSA Processing Considerations

SWIR1 contrast between land and water was generally good. Terrain shading of land pixels whose elevation was below the elevation threshold was only a significant issue for a Landsat 8 OLI image acquired on 12/14/2013. For this image only, any identified water pixel must also have been identified on the previous image in the time series (acquired on 10/11/2013), when the reservoir was 5 feet higher.

Sun glint on any of the 22 selected Landsat images was rarely severe, so a 6% reflectance threshold was adequate to identify all 100% water pixels on all but two Landsat scenes. Reflectance threshold of 8.5% and 6.5% were used for the images acquired on 6/21/2013 and 6/8/2014, respectively.

Lake Cachuma is located near the center of Landsat WRS2 (World Reference System2) path 42, which allowed for the use of Landsat 7 ETM+ images that were acquired after the scan-line corrector failure on 5/31/2003. ETM+ images acquired after 5/31/2003 contain a continuous swath of imagery along the satellite's nadir path, but wedges of no-data appear on either side and increase in size as they approach the eastern and western edges of the image swath. Only small slivers of no-data occurred on a few of the ETM+ images of Lake Cachuma. On these images, successive 3x3-pixel moving average filters were applied to the imagery that replaced no-data pixels with the mean values from their immediate neighbors. The result of this operation can be seen in Figure 3.

Area and Volume Calculations

A significant, monotonic drawdown at Lake Cachuma occurred between 2011 and 2016, allowing for image acquisitions to record the location of a steadily receding shoreline over a fairly short time period (Figure 4). Landsat estimates of mean reservoir surface area and reservoir volume between 650' and 750' are 1.1% and 1.0% less than those calculated from the 2013 survey data (Table 2). The mean RSA value generated from images acquired prior to the survey is 2.1% less than that generated from the survey data, while the mean RSA value generated from images acquired after the survey is nearly identical (0.1% greater) than the mean value generated from the survey data (Figures 5 and 6). Landsat-derived volume generally follows the trend of diminshing reservoir capacity established by the two reservoir surveys in 1989 and 2013 (Figure 7).

Lake Mead, AZ/NV

Approximate surface area at full pool:	158,000 acres
Approximate full pool elevation:	1221 ft
Max. SWIR1 reflectance threshold:	12%
Max. DEM elevation threshold:	1214 – 1234 ft (370 to 376 m)
Date range of image acquisitions:	March 2000 – September 2016
Closest in time reservoir surveys:	2001 (full survey) September 2009 (LiDAR only above 1095' reservoir elevation)

Lake Mead began filling in 1936 after the completion of Boulder Dam (later renamed Hoover Dam), which is located about 6 miles northeast of Boulder City, Nevada (Figure 8). It extends more than 70 miles upstream of Hoover Dam through the Mojave Desert of Nevada and Arizona and into the lower reaches of the Grand Canyon. It is the largest reservoir by volume in the Colorado River system. Desert scrub vegetation and bare rock/soil compose most of its shoreline, except at tributary inflows where riparian and/or agricultural vegetation exists. Lake Mead is managed to provide water storage, flood control, hydroelectric power, and recreation.

RSA Processing Considerations

The accuracy of water proportion estimates along the shoreline of Lake Mead is enhanced by the generally high contrast between the highly reflective land surfaces and the dark water. Although terrain shading was concern for a few areas of the reservoir where steep cliffs go down to the water's edge, the DEM elevation threshold prevented nearly all shadow pixels from being identified as water.

Strong desert winds blowing over long fetches on Lake Mead can produce large waves which, when combined with high sun angles, often produce severe sun glint. Severe glint occurred on several of the processed images, so the SWIR1 reflectance threshold had to be set to a very high 12% to effectively identify all water pixels on all images. Fortunately, SWIR1 reflectance of the mostly bare soil and rock shoreline of Lake Mead commonly approached 40%, so there was ample contrast between even the brightest water pixels and adjacent land. The higher SWIR1 reflectance threshold had the added benefit of allowing the identification of some of the narrow flooded canyons along the perimeter of Lake Mead that would have been missed with a lower SWIR1 threshold.

Visual cues for accurately determining the transition line between the Colorado River and Lake Mead at the far eastern end of the reservoir were largely missing from the Landsat imagery, making an accurate delineation of the reservoir/river boundary impossible. Figure 9 shows the Colorado River inflow area from two images that document reservoir elevations of 1149.01 (left) and 1143.04' (right). The upper panels contain just the color Landsat (NIR, red, green = R, G, B), while the bottom images contain the same Landsat image rendering overlaid with the water proportion image color-coded from blue (100% water) to red (0% water). The turquoise waters of the sediment-laden Colorado River are clearly seen on both of these images, but the precise location of the river/reservoir boundary is not obvious. However, due to the large size of Lake Mead relative to the Colorado River, the uncertainty resulting from indistinct reservoir boundaries at the Colorado River inflow downstream of the Grand Canyon appeared to be less than 0.25% in most cases.

Due to their relatively high SWIR1 reflectance values, boat marinas were identified as land by the automated RSA mapping procedure. These areas were manually identified on the Landsat images documenting the 12 highest reservoir elevations, and the water proportion values for all identified pixels were set to 1.0. The average increase in reservoir area resulting from this procedure was 54.5 acres. To save time, 54.5 acres was added to the automatically-derived RSA values for the remaining 18 RSA maps.

Accurate delineation of the reservoir boundary became even more difficult as the reservoir backed up into the narrow confines of the lower Grand Canyon. For the four images of Lake Mead where this occurred (with lake elevations exceeding 1197 feet), the upper end of Lake Mead along the Colorado River was arbitrarily set to be where the Colorado River exits the Grand Canyon at the Grand Wash Cliffs near the eastern end of the lake (Figure 8).

Area and Volume Calculations

Lake Mead experienced a long period of generally decreasing elevations between 2000 and 2010, during which time most of the Landsat images used in this analysis were acquired. Reservoir elevations rebounded somewhat in 2011 and early 2012, but then resumed a general downward trend to a minimum of 1072' that occurred in July, 2016 (Figure 10).

Landsat RSA measurements from the same year as the 2001 and 2009 reservoir surveys closely matched the RSA values produced from the survey data (Figures 11-13). The mean RSA measured from the four Landsat images acquired in 2001 was within 0.05% of that calculated using the 2001 survey data (130,929 and 130,993 acres, respectively); and the mean RSA from the three Landsat images acquired in 2009 was within 0.18% of that derived from the 2009 LiDAR survey data (88,766 and 88,929 acres, respectively). But differences between image-based and survey-based RSA estimates increased for non-survey years.

Differences in Landsat- and survey-derived RSA for the four images acquired in 2000 (identified in red bold type in Figure 11) can be explained by the fact that the image-based estimates came from RSA maps that set the upper end of the reservoir at the beginning of the Grand Wash Cliffs near the eastern edge of Figure 9. The survey data cotinued up the Colorado River into the Grand Canyon, so RSA estimates calculated from these data were understandably larger.

Looking at the 2001 survey data in Figure 12, image acquisitions from 5/1/2002 onward also produced smaller RSA estimates than the 2001 survey data. Although some of these differences can be explained by the transport of previously deposited sediment in the upper reaches of the reservoir downstream in subsequent years, a significant portion appears to have arisen from differences between how the two methods define reservoir extent. The survey-based RSA estimates come from a GIS method that 'slices' a terrain model generated from the survey data at the defined reservoir elevation and includes all areas that are at or below the specified elevation as part of the reservoir, including isolated pools and the river channel itself upstream of the main reservoir. The image-based RSA are more tightly constrained by analyst-defined polygons that define the boundaries between tributaries and the reservoir. About 40% of the sudden decrease in image-measured RSA relative to 2001 survey-based RSA on 5/1/2002 can be attributed to the exclusion of Grand Wash Bay (the first significant bay to the north of the Colorado River's channel after it exits the Grand Canyon) from all Landsat-based RSA measurements from 5/1/2002 onward (see upper right corner of Figure 9). Numerous other smaller isolated ponds along the floodplain of the Colorado River upstream of Grand Wash Bay were excluded as well.

The effect of sediment transport is even more pronounced in Figure 13, which compares RSA estimates from Landsat and the 2009 LiDAR-based survey. This survey only mapped the areas of Lake Mead above the 1095' reservoir elevation that were exposed at the time of LiDAR data acquisition. Because there had been a fairly steady drawdown in reservoir elevation from 2000 to 2009, much of the sediment in the upper reaches of the reservoir had been transported down-reservoir during that time period. Because the Landsat images were acquired before that transport had occurred, the RSA values were smaller than the RSA estimates generated from the 2009 LiDAR data, after sediment had been transported downstream. The greater the time difference between image acquisition and the 2009 LiDAR survey, the greater the difference was between Landsat- and survey-derived RSA values.

Landsat estimates of mean reservoir surface area and reservoir volume between 1080' and 1190' are 1.0% less than that calculated from the 2001 survey data, and 2.1% less than that calculated from the 2009 LiDAR survey data (Table 2). Given the close match of Landsat- and survey-derived RSA estimates when image acquisition dates matched survey dates, the majority of the observed differences can be attributed to the factors described above: erosion, downstream transport, and redeposition of sediments in the upstream portions of the reservoir as reservoir elevations fell, and off-channel impoundments being included in the survey-based estimates but not in the Landsat-based estimates. But notwithstanding those differences, Landsat-derived volume estimate generally follows the trend set by the five reservoir surveys that have been performed on Lake Mead (Figure 14).

Elephant Butte Reservoir, NM

Approximate surface area at full pool:	36,500acres
Approximate full pool elevation:	4409 ft
Max. SWIR1 reflectance threshold:	10%
Max. DEM elevation threshold:	4364 – 4462 ft (1330 to 1360 m)
Date range of image acquisitions:	March 1998 – September 2004
Closest in time reservoir survey:	March – April, 1999

Elephant Butte Reservoir is located along the Rio Grande River in the high desert of southern New Mexico. The reservoir forms behind Elephant Butte Dam, which is located 4 miles northeast of Truth or Consequences, New Mexico (Figure 15). Desert scrub vegetation and bare rock/soil compose the majority its shoreline, except at the inflow of the Rio Grande River where riparian vegetation exists. Elephant Butte Reservoir is managed primarily for irrigation, but also provides flood control, hydroelectricity, and recreation.

RSA Processing Considerations

Contrast between land and water was generally good at Elephant Butte, with the bright desert soils contrasting strongly with the dark water. Sun glint was a significant factor at this reservoir as well, but a maximum SWIR1 reflectance value of 10% was adequate to identify all glint-affected water pixels in all processed Landsat scenes. This reflectance threshold was reduced to 9% for a Landsat 8 OLI image acquired on 12/31/2013, because the low sun angle on this date essentially eliminated sun glint, and because the low local sun angles on the banks of the reservoir that faced away from the sun during image acquisition reduced their apparent SWIR1 reflectance, reducing the contrast between land and water.

Terrain shading of the banks of the reservoir was limited to only a few locations along the eastern shore of the reservoir on images acquired when sun angles were low. The shaded areas were manually excluded using manually-delimeated AOI polygons. Defining the reservoir boundary was sometimes difficult, but the transition zone was better defined than the Colorado River inflow to Lake Mead.

Boat marinas were identified as land by the automated RSA mapping procedure. The RSA map developed from each Landsat image was manually modified to show all marina areas as 100% water.

Area and Volume Calculations

Elephant Butte Reservoir experienced a rapid drawdown from January 2000 through September 2003, but images from 1998 to 2004 were processed to document the largest possible range of reservoir elevations (Figure 16).

Agreement between the remotely sensed and survey-derived RSA values was very good, probably due to the close temporal proximity of the two datasets (Figures 17 and 18). The mean RSA value from all 21 image acquisition dates agreed with the mean survey-derived values for the same reservoir elevations to within 0.2%, as did estimates of reservoir volume between 4300’ and 4400’ reservoir elevation.

Landsat estimates of mean reservoir surface area and reservoir volume between 4300’ and 4400’ are 0.2% less than that calculated from the 1999 survey data (Table 2). Figure 19 shows close agreement between reservoir volume estimates between elevations 4300 and 4400 feet derived from 1999 and 2007 reservoir surveys, and the 1998 – 2004 Landsat imagery.

Black Canyon Reservoir, ID

Approximate surface area at full pool:	1,090 acres
Approximate full pool elevation:	2498 ft
Max. SWIR1 reflectance threshold:	6%
Max. DEM elevation threshold:	2520 ft (768 m)
Date range of image acquisitions:	October 2002 – November 2002
Closest in time reservoir survey:	2016

Black Canyon Reservoir is created by Black Canyon Dam on the Payette River in western Idaho, approximately 25 miles north of Boise (Figure 20). The dam was originally completed in 1924, then re-constructed between 1951 and 1955. Black Canyon is a relatively small diversion reservior, whose purpose is to divert water to the Black Canyon and North Side Main irrigation canals. Consequently, the reservoir remains full for the entire irrigation season, allowing a narrow strip of riparian vegetation to exist in an otherwise arid rangeland setting. An expansive wetland complex is located at the upper end of the reservoir, and intermittantly-irrigated pasture is also found in the hills above the reservoir’s southern shoreline.

RSA Processing Considerations

Because Black Canyon is a diversion reservoir it is kept full during the irrigation season, it is only drawn down for maintenance which normally occurs during the late fall or winter months. Only five Landsat images could be acquired to map RSA during a brief drawdown period during the fall of 2002. Consequently, elevation differences between image acquisitions were larger than for the other reservoirs in this study.

Low sun angles during image acquisition prevented significant sun glint from occuring on any of the Landsat images. However, the rugged topography surrounding the reservoir combined with the low sun angles present during three of the five image acquisitions to produce terrain shading problems along the southwest shore of the reservoir from about 0.6 to 1.6 miles upstream of the dam. For the affected images, AOI polygons were manually drawn to define the shoreline for the shaded portion of the reservoir’s perimeter.

The uncertain definition of the river/reservoir boundary was by far the most significant factor affecting RSA estimates at Black Canyon Reservoir. The estimate of the reservoir's upstream extent on each image was done using only commonly available datasets, such as USGS topographic maps and the satellite images themselves. Cues on the imagery included the location at which sun glint or whitewater from riffles ceased, the location at which water depth noticably increased (as seen by darker tones in the visible and near infrared bands) or - at maximum reservoir elevaiton - the location at which changing rivier inflow discharges over the course of the spring and summer did not affect shoreline location.

Area and Volume Calculations

The elevation profile of Black Canyon Reservoir shows that it is kept full during the irrigation season, with occasional drawdowns for maintenance (Figure 21). All five Landsat images used to map RSA were acquired between 10/6/2002 and 11/30/2002. This is the ideal case where surface areas can be measured over a wide range of reservoir elevations in a relatively short time period (week compared to decades).

Figure 22 shows that sedimentation has significantly reduced the areal extent of Bighorn Reservoir between the two survey dates of 1983 and 2016. There is reasonable agreement between the 2002 remotely sensed and 2016 survey-based estimates of RSA (Figures 22 and 23), but results are somewhat counterintuitive, with 2002 RSA values being slightly smaller than 2016 values for three of the five images. This is not surprising however, given the difficulty in defining where the reservoir ends and the river begins.

Landsat estimates of mean reservoir surface area and reservoir volume between 2465.3' and 2497.5' are 0.7% and 1.8% less (respectively) than those calculated from the 2016 survey data (Table 2). Such close agreement probably indicates error in the Landsat-based RSA numbers because we would expect more sediment to have been deposited in 2016 than in 2002. RSA errors from the satellite imagery most likely arise from uncertain definition of the reservoir/tributary river boundary.

Paonia Reservoir, CO

Approximate surface area at full pool:	330 acres
Approximate full pool elevation:	6253 ft
Max. SWIR1 reflectance threshold:	6%
Max. DEM elevation threshold:	6463 ft (1970 meters)
Date range of image acquisitions:	October 2010 – August 2018
Closest in time reservoir surveys:	2013, 2015, 2016

Paonia Reservoir is a storage reservoir located on the North Fork of the Gunnison River in western Colorado, 14 miles east northeast of Paonia, Colorado (Figure 25). Paonia Reservoir is impounded by Paonia Dam, which was completed in 1962. There has been significant sedimentation and loss of water storage volume within the reservoir since its construction. Oakbrush and sagebrush with scattered conifers dominate the rugged landscape surrounding the reservoir, with coniferous forests occuring on north-facing slopes.

RSA Processing Considerations

For the reservoirs previously described, the difference in SWIR1 reflectance between water and nearby land pixels was great enough that the selected SWIR1 threshold would identify all water pixels and a ring of shoreline pixels that were composed primarily of water, but contained a minority fraction of land. At Paonia Reservoir however, low local sun angles at forested locations combined with shadowing from individual trees within the forest to produce SWIR1 reflectance values of around 10% - not significantly greater than the 6% threshold used to identify water. Consequently, the proportion of land in some of the initially-identified water pixels was greater than 50%, and performing the usual buffering procedure to identify the additional layer of shoreline pixels led to an over-identification of shoreline pixels. Fortunately, the coniferous forests produced a high NDVI value of about 0.75, which strongly contrasted with the negative NDVI values most often associated with open water. To reduce commission errors along the eastern perimeter of Paonia Reservoir, any pixel with an NDVI value greater than zero was excluded from the initial water mask prior to its expansion to identify the second layer of shoreline pixels.

Shading from terrain became an issue in the autumn and winter months as sun angles at the time of Landsat image acquisition decreased. For images acquired during these months, AOI polygons were carefully drawn along the shoreline in shaded areas, effectively overriding the automated water surface mapping procedure with visual image interpretation.

Defining the boundary between the reservoir and its tributary stream was simpler for Paonia Reservoir than the other reservoirs in this study, but its small size made any errors in boundary definition more consequential as a proportion of total reservoir surface area.

Area and Volume Calculations

Figure 26 shows the reservoir elevation graph for Paonia Reservoir and the acquisition dates of images used to measure RSA. Images were acquired over a seven year span between 2010 and 2018 to ensure an approximate 5-foot reservoir elevation difference between successive RSA measurements. Because of the small size of Paonia Reservoir, observed increases in reservoir elevation during the spring runoff period approached 3 feet per day. Such rapid elevation change made the use of a daily reservoir elevation (as was done for the other reservoirs in this study) problematic. For Paonia reservoir, reservoir elevation at the time of the Landsat overpass was obtained from 15-minute elevation data.

Agreement between imagery-based and survey-based RSA estiamtes are reasonable, but imperfect (Figures 27 - 29). It is not surprising that the two largest outliers come from images that are among the furthest in time from the 2016 reservoir survey. Correlation between the satellite-measured and survey-derived RSA values improves if satellite-measured values are compared to the survey-derived values that are closest to them in time, but the improvement is minor (Figure 29).

Landsat estimates of mean reservoir surface area and reservoir volume between 6370' and 6448' are 2.1% and 1.4% less, respectively, than those calculated from the 2016 survey data (Table 2). Landsat-derived volume is below the trend of diminshing reservoir capacity established by the four reservoir surveys performed in 1988, 2013, 2015, and 2016 (Figure 30).

Bighorn Lake, MT/WY

Approximate surface area at full pool: 17,300 acres
Approximate full pool elevation: 3657 ft
Max. SWIR1 reflectance threshold: 6%
Max. DEM elevation threshold: 3740 ft (1140 m)
Date range of image acquisitions: October 2010 – August 2018
Closest in time reservoir survey: July, 2007

Bighorn Lake is located along the Bighorn River in Montana and Wyoming. It is impounded by Yellowtail Dam (completed in 1967) located near Fort Smith, Montana, about 42 miles southeast of Billings Montana (Figure 31). The reservoir provides flood control, power generation, irrigation, and recreation. The upper 25% of the full-pool reservoir is located in open, arid rangeland. The remainder falls within the steep-walled Bighorn Canyon, which cuts across the northern end of the Bighorn Mountains. The canyon is more than 2000 feet deep in places, and the shoreline here is composed primarily of steep rock walls and areas of sagebrush.

RSA Processing Considerations

Sun glint conditions were never extreme on Bighorn Lake, so a SWIR1 reflectance threshold of 6% was effective at identifying all water pixels in the reservoir.

As was seen at Paonia Reservoir, the rugged terrain surrounding Bighorn Lake produced numerous locations around the perimeter of the reservoir where the sun at the time of Landsat image acquisition was only a few degrees above the local horizon, producing minimal contrast between the land and reservoir. But unlike Paonia reservoir, the deep canyon environment at Bighorn Lake produced numerous locations where water, shoreline, and adjacent land pixels were all in terrain shadow. These conditions existed on all Landsat images, even those acquired in late spring and early summer with the highest sun angles, but were more numerous on the images acquired earlier in the spring or later in the summer or early autumn when sun angles were lower. An NDVI threshold was not used to aid the identification of water pixels at Bighorn Reservoir as it was with Paonia Reservoir because setting the NDVI threshold low enough to exclude all shaded land areas would have excluded water pixels experiencing moderate sun glint, and areas of inundated vegetation at the upper end of the reservoir.

In low-illumination and shaded areas of the reservoiir, a rasterized version of the Bighorn Lake polygon present in the National Hydrographic Database (NHD) was used to estimate reservoir extent. The steep canyon walls where terrain shading was an issue usually meant that incremental changes in reservoir elevation resulted in only minor changes in reservoir surface area. And given that less than 10% of the reservoir's perimeter was shaded on the image with the lowest sun angle at image acquisition, the error in surface area measurment was considered to be relatively minor. It should be emphasized that the rasterized reservoir extent from the NHD was used only to define reservoir pixels in shaded and low-illumination areas, so if a narrow portion of the reservoir was too small to be identified as water by the initial SWIR1 thresholding procedure, it was not identified in the final RSA image map. This meant that portions of narrow side canyons of Bighorn Lake were not included in the RSA estimates, despite being present in the NHD.

Operationally, the 'Hillshade' tool in ArcGIS was used to generate masks of shaded and low sun angle areas where a rasterized version (30-meter grid spacing) of the Bighorn Reservoir polygon in the NHD was used to define the reservoir's extent. The Hillshade tool generated images of local solar illumination values for each Landsat image from a 30-meter digital elevation model and the solar elevation and azimuth values at the time of image acquisition. Output solar illumination values consist of the cosine of the local solar incidence angle (measured relative to surface normal) scaled to fill the 8-bit (0 to 255) data range. A pixel was identified as a shaded or low-illumination pixel if its local solar illumination value was less than a quarter of that of a sunlit flat, level surface.

Although the Bighorn River was flowing into the reservoir during every Landsat image acquisition, determining the beginning of the reservoir was not as difficult as it was for Lake Mead and Elephant Butte Reservoir. However, determining where the river ended and the reservoir began in the flat, marshy area upstream of Bighorn Canyon was subjective. In this area, the upper end of the reservoir was defined as the location at which water became visible in the floodplain beyond the riparian vegetation that bordered the river in most locations. The SWIR1 thresholding was allowed to operate in these areas, producing a non-homogeneous surface or water proportions that appears to accurately represent actual conditions (Figure 32).

Area and Volume Calculations

Bighorn Lake reached a low elevation of 3573 feet in March of 2003, only 26 feet above the elevation of inactive storage in the reservoir. The reservoir gradually refilled over the next seven years. Landsat images were acquired within this time period to document the rise in reservoir levels, but additional images acquired in 2016 – 2018 were processed as well to fill in significant elevation gaps in the 2003 – 2011 image dataset (Figure 33).

Agreement between RSA estimates generated from Landsat imagery and the 2007 reservoir survey are reasonable (Figures 34 and 35), but contain six significant outliers, which are highlighted in bold type in Figure 34. Inspection of the reservoir survey data and the associated survey report (Ferrari, 2010) offer an explanation for these outliers. A multibeam echosounder was used to acquire the vast majority of the bathymetry data within Bighorn Canyon, but a single-beam depth sounder was used exclusively in the portion of the broad floodplain at the upper end of Bighorn Lake below about 3629' elevation, where three of the significant outliers exist. The survey report describes calibration problems with the single-beam depth sounder at the upper end of the reservoir (which was between 3635.7' and 3637.5' elevation during the survey). The instrument was calibrated by lowering a weighted marked cable and comparing the cable depths to digital depths. The survey report states: "In the upper portion of the reservoir in the deeper portion of the channel, the sediment laden bottom was very soft, allowing the weight to easily sink 1 to 2-feet below the reservoir bottom, making accurate calibration difficult."

The ramifications of this calibration error can be seen in Figure 36, where the 3610-foot contour derived from the 2007 reservoir survey data is overlaid onto the 5/15/2018 Landsat image, acquired at a reservoir elevation of 3610.04 feet. The 3610-foot contour generated from the survey data extends far above the high water line visible in the image, and also extends about 6 miles up the channel of the Bighorn River, adding about 300 acres to the calculated reservoir surface area. The surveyed RSA for 3610.04' is 360 acres larger than the image-based estimate, so the ~300 acre overestimation accounts for more than 80% of the observed difference. This example indicates that the RSA values derived from the survey data are probably overestimates of the actual values in the elevation range that depended exclusively on single-beam depth sounder data (~3610' to 3629').

The other significant outliers are the estimates for the three highest reservoir elevations captured by Landsat imagery. No hydroacoustic bathymetry data were acquired above about 3629', and no topographic data above that elevation were derived from new photogrammetric or LiDAR data. Consequently, bathymetry above the 2007 survey data came from elevation contour data from the original USGS topographic maps used for the initial reservoir volumetric analysis, and from high-altitude aerial imagery acquired in 2004, 2006, and 2009 that was used to digitize reservoir perimeters between 3586' and 3644'. The survey report states: "Even with multiple data sources, the 2007 developed contours were very crude in the upper elevation contours and small coves of the reservoir." The image-based RSA underestimates relative to the survey-derived data at the three highest reservoir elevations might have resulted from unmapped reservoir sedimentation that occurred in the upper end of the reservoir since its construction in the 1960s.

The remaining image-based RSA data correlate well with the RSA data derived from the reservoir suvey data. Using the Bighorn Lake boundary from the NHD to estimate the lake perimeter in shaded areas of the reservoir had a minimal effect on results. Average RSA of the remaining 12 images (7306.9 acres) was 0.8% less than the values derived from the 2007 survey data (7661.3 acres). Figure 37 shows that the Landsat-based estimate of reservoir volume between 3575' and 3655' closely follows a linear trend established by the first two surveys completed in 1965 and 1982. However, primarily for the reasons discussed above, Landsat estimates of mean reservoir surface area and reservoir volume between 3575' and 3655' are 2.1% and 2.4% less, respectively, than that calculated from the 2007 survey data (Table 2).

It should be mentioned that although reservoir volume was assessed for only an 80-foot thick 'slice' of Bighorn Reservoir that has a maximum depth of approximately 500 feet, the 640,402 AF contained within that 'slice' is 50% of the total reservoir volume reported by the 2007 survey, and 79 percent of its live storage (469910 AF is considered inactive storage).

Combined Data from All Reservoirs

The sum of all Landsat-derived reservoir surface area estimates for the five reservoirs for which a reservoir survey was performed within the time window of Landsat image acquisitions is 0.9% less than the summed surface area estimates derived from the reservoir survey data. If the comparison is limited to data from imagery acquired within one year of a reservoir survey, the difference is reduced to 0.5%.

Documenting Reservoir Surface Area Change over Time

The work described above shows how RSA maps from multitemporal images can be used to estimate reservoir storage between the highest and lowest reservoir elevations present in the image set. For this application, it is best to acquire the image data in as short a time period as possible to minimize changes in reservoir bathymetry between image acquisitions. But satellite-based RSA measurements can also be used to document changes in reservoir surface area at a single reservoir elevation over time. Figures 38 – 40 show the process of sedimentation occurring at three different elevations of Elephant Butte Reservoir (4329.1', 4320.9', and 4311.6'). Figure 41 plots the calculated RSA values over time for each reservoir elevation. All three image sets show a reduction in RSA over time, but the rates at which this reduction takes place varies from near linear for elevation 4320.9 to decidedly non-linear for elevations 4311.6 and 4329.1.

Discussion

This report describes a method to calculate reservoir surface areas from Landsat imagery, and describes how these measurements can be combined with reservoir elevation data to estimate reservoir volume between the lowest and highest reservoir elevations represented by the Landsat image set. Although the calculation of water percentages from Landsat imagery is done using a set of image processing steps that have been combined into a single model in the ERDAS Imagine software package, the procedure is not fully automated. Analyst time is still needed to:

- acquire reservoir elevation data and define time periods of interest,
- select and obtain cloud-free images during those time periods, while avoiding Landsat 7 ETM+ images which exhibit wide (> 3 pixels) data gaps over the reservoir,
- if necessary, fill Landsat 7 data gaps using spatial filtering,
- acquire a suitable DEM of the study area and resample it into the map projection used by the satellite imagery (a 1 arc second NED DEM was used for this study),
- define DEM thresholds that will prevent shaded terrain from being identified as water,
- define an 'area of interest' polygon around the reservoir on each image that defines the area to be processed, taking care to accurately define the reservoir boundary at tributary inflow areas and along shaded regions of the shoreline,
- inspect the imagery to select a SWIR1 threshold that is adequate to identify the vast majority of open water pixels in the image, and
- once automated processing is complete, manually identify and fill in occasional misclassifications caused by severe sun glint, boat marinas, bridges, and other high reflectance targets on the reservoir.

Both reservoir surface area and reservoir volume estimates between the lowest and highest reservoir elevations for which Landsat imagery is available agree closely to values obtained from conventional reservoir surveys. Summed reservoir surface area estimates for all processed images is 0.9% less that survey-derived values. If the dataset is restricted to imagery acquired within one year of the reservoir survey against which its data are compared, the difference is reduced to 0.5%. The results suggest that this method could be used for preliminary assessment of reservoir storage volume changes over time.

Input Imagery

The linear mixture model that is used to assign water proportions to pixels along the shoreline of the reservoir is not necessary when using high-resolution (i.e., ~3m or smaller pixel size) aerial or satellite imagery to map RSA. However, the linear mixture model is necessary when using moderate resolution imagery like that from the optical sensors aboard the Landsat satellites (30 m pixel size). The linear mixture model allows for accurate RSA estimates for small reservoirs down to a few tens of acres in size to be generated from Landsat imagery.

Although Landsat imagery was used exclusively for this project, it is not the only choice for imagery from which RSA can be measured. There are numerous spaceborne optical sensors that offer better temporal and/or spatial resolution than Landsat. The Disaster Monitoring Constellation provides imagery with a 30 meter pixel spacing, 373 mile swath width, daily repeat imaging, and green, red, and NIR spectral bands. The Sentinel 2A and 2B satellites operated by the European Space Agency (ESA) provide imagery with a 10 meter pixel size, 180 mile swath width, an approximate 5-day repeat cycle, and visible, NIR, and SWIR spectral bands. Numerous vendors also offer high-resolution satellite imagery (< 5 meter pixel spacing) in the visible and near infrared wavelengths. However, there are drawbacks associated with high-resolution imagery, including:

- image acquisition usually needs to be scheduled,
- continuous imagery of large reservoirs like Lake Mead cannot always be acquired on the same day,
- there can be image licensing requirements, and
- orthorectified, atmospherically corrected images typically are not standard products.

The main benefit of using Landsat imagery is that there is a continuous image record with 8-day to 16-day repeat coverage going back to 1984 that is available free of charge to everyone. This allows retrospective viewing of reservoirs anywhere in the world back to 1984 – something not offered by any other moderate- or high-resolution image source. In addition, the 115 mile swath width of the Landsat sensors is large enough to capture all but the largest reservoirs on a single image swath, while the nadir-viewing sensors with a relatively narrow (±7 degree) field of view reduce the probability and severity of sun glint compared to sensors with wider look angles. Finally, important image post-processing is routinely applied to Landsat imagery free of charge, including orthorectification and radiometric calibration to either spectral radiance, TOA (top of the atmosphere) reflectance, and/or apparent surface reflectance. Such processing ensures consistent results from consistent model parameters that is not possible from uncalibrated images.

Factors Affecting Reservoir Surface Area Estimates

The method functions properly under most sunlit conditions, as long as the SWIR1 reflectance of the land adjacent to the reservoir is above the SWIR1 reflectance threshold used to initially identify water pixels. Where this is not the case (typically in shaded or low incidence angle conditions), automated definition of the land/water boundary and calculation of water proportion for shoreline pixels becomes impossible. Under these circumstances, the image analyst must define the reservoir boundary, either through manual digitizing or through substitution of another reservoir boundary dataset.

The SWIR1 thresholds used to initially identify water pixels in this study ranged from 6% to 12%. The magnitudes of the thresholds were determined by the severity of sun glint seen in any of the Landsat images being processed for any given reservoir. It should be noted that increasing the SWIR1 threshold has the effect of identifying more water pixels, leading to an increase RSA values. The effect of increasing SWIR1 thresholds on final RSA estimates depends primarily on the area to perimeter ratio of the reservoir, but the SWIR1 reflectance of the land pixels adjacent to the shore pixels has an effect as well. Limited tests showed that a 1% increase in the SWIR1 threshold value applied to Lake Cachuma (maximum measured RSA of 2982 acres) from 6% to 7% increased reservoir surface area and reservoir volume estimates by 0.3%, while twice that increase (2%) in SWIR1 threshold value applied to the larger Elephant Butte Reservoir (maximum measured RSA of 34,205 acres) produced the same 0.3% increase in both values.

Some of the observed differences between the remotely sensed and survey-derived RSA values in this study almost certainly resulted from imagery being acquired over a multi-year period, during which time overall sediment volume in the reservoir increased, and sediments deposited in previous years were redistributed. Users of this method need to be aware of the inevitable changes to sediment quantity and distribution within a given reservoir over the time period of image acquisition.

The model described in this report could be modified slightly if necessary to improve RSA estimates; but doing so requires a reliable ground truth dataset against which to compare Landsat-based RSA estimates. A set of orthorectified, high-resolution aerial or satellite images of reservoirs of different sizes that were acquired near the same time and near the same reservoir elevation as available Landsat imagery could provide such a dataset.

Landsat Dynamic Surface Water Extent Product

In February of 2019, the USGS (U.S. Geological Survey) released a new Level-3 Science Product called Landsat DSWE (Dynamic Surface Water Extent) (Jones, 2019). The DSWE product package contains six acquisition-based raster products pertaining to the existence and condition of surface water. Intermediate bands used to produce the DSWE product are also provided. The 'interpreted layer' (one of the six raster products) classifies pixels into five classes:

- Not water,
- Water – high confidence,
- Water – moderate confidence,
- Potential wetland, and
- Water or wetland – low confidence.

This product became available after most of the image processing for this project was complete, and was therefore not evaluated for its utility in estimating RSA. Future work should evaluate this product as it is routinely produced and available free of charge from the USGS at https://earthexplorer.usgs.gov/.
More information can be found at: https://www.usgs.gov/land-resources/nli/landsat/landsat-dynamic-surface-water-extent.

Conclusions

The most useful applications of this method are to determine area and capacity curves for reservoirs, and to monitor change in reservoir surface area over time at the same water surface elevation.

During this project, an average of about 7 staff days per reservoir was used to develop area and capacity curves for each reservoir. But this included initial development time, and time for studying reservoir survey reports and data to understand potential reasons for observed differences between image- and survey-based results. Future work of similar quality using the model developed in this project could be accomplished more quickly in the future, probably about 5 staff days per reservoir. Processing times could be shortened further to 3 or 4 days per reservoir if there is more tolerance for error in model results. Much of the time in the model runs this time was spent pursuing solutions to problems that probably did not alter RSA estimates by more than a percent or two. It should be emphasized that for determining area and capacity curves, obtaining imagery from the narrowest possible date range will produce the best approximation to the 'snapshot in time' produced by conventional reservoir surveys. A narrow date range limits the accumulation of new sediments and the redistribution of existing sediments during the measurement period.

Staff days needed to monitoring reservoir surface area over time depends on the number of images processed. If a cloud-free image of a given reservoir is not available at a precise desired reservoir surface elevation at a given point in time, but recently acquired images document elevations above and below the target elevation, linear interpolation of surface areas between the two good images will produce useable results. The processing cost for a longitudinal survey of RSA over time will of course depend on the number of images processed, but a reasonable estimate of processing time for a 10-date time series (i.e., up to 20 processed images) would be approximately the same (5 days) as the time needed to develop an area capacity curve for a reservoir.

References

Abileah, R., S.Vignudelli, and A. Scozzari (2011) A completely remote sensing approach to monitoring reservoirs water volume. *International Water Technology Journal* 1:63–77.

Arsen, Adalbert, Jean-Francois Cretaux, Muriel Berge-Nguyen, and Rodrigo Abarca del Ril, 2014. Remote Sensing-Derived Bathymetry of Lake Poopo, *Remote Sensing* 2014, 6, 407-420, doi 10.3390/rs6010407.

Duan, Zheng and W.G.M. Bastiaanssen, 2013. Estimating water vossen, 2013; lume variations in lakes and reservoirs from four operational satellite altimetry databases and satellite imagery data, *Remote Sensing of Environment* 134:403-416, doi:10.1016/j.rse.2013.03.010.

Ferrari, Ronald L., 2010. *Bighorn Lake - Yellowtail Dam 2007 Sedimentation Survey,* U.S. Bureau of Reclamation Technical Report No. SRH-2010-12, 113 pp.

Gao, Huilin, Charon Birkett, and Dennis P. Lettenmaier, 2012. Global monitoring of large , reservoir storage from satellite remote sensing, *Water Resources Research* Vol 48, Issue 9, 12 pp., W09504, doi:10.1029/2012WR012063.

Jones, J.W., 2019. Improved Automated Detection of Subpixel-Scale Inundation—Revised Dynamic Surface Water Extent (DSWE) Partial Surface Water Tests. *Remote Sensing*, *11*, 374 https://doi.org/10.3390/rs11040374.

Liu J, Z. Wang, T. Gong , and T. Uygen, 2012. Comparative analysis of hydroclimatic changes in glacier-fed rivers in the Tibet and Bhutan-Himalayas, *Quaternary International* 282:104–112.

McFeeters, S. K., 1996. The use of the Normalized Difference Water Index (NDWI) in the delineation of open water features, *International Journal of Remote Sensing*, 17:7, 1425-1432, DOI: 10.1080/01431169608948714.

Ricko, M., CM Birkett, JA Carton, and J-F Cretaux, 2012. Intercomparison and validation of continental water level products derived from satellite radar altimetry, *Journal of Applied Remote Sensing* 6(1), 061710 (12 December 2012). https://doi.org/10.1117/1.JRS.6.061710.

Roman, Uday C., Jatwa Suneeta, M. N. Singh, and S. Selvan, 2010. Reservoir Capacity Loss Estimation Using Satellite Data – A Case Study, *Indian Geotechnical Conference – 2010, GEOtrends,* December 16-18, 2010. IGS Mumbai Chapter & IIT Bombay.

Xu, Hanqui, 2006. Modification of the normalised difference water index (NDWI) to enhance open water features in remotely sensed imagery, *International Journal of Remote Sensing*, 27:14, 3025-3033, DOI: 10.1080/01431160600589179.

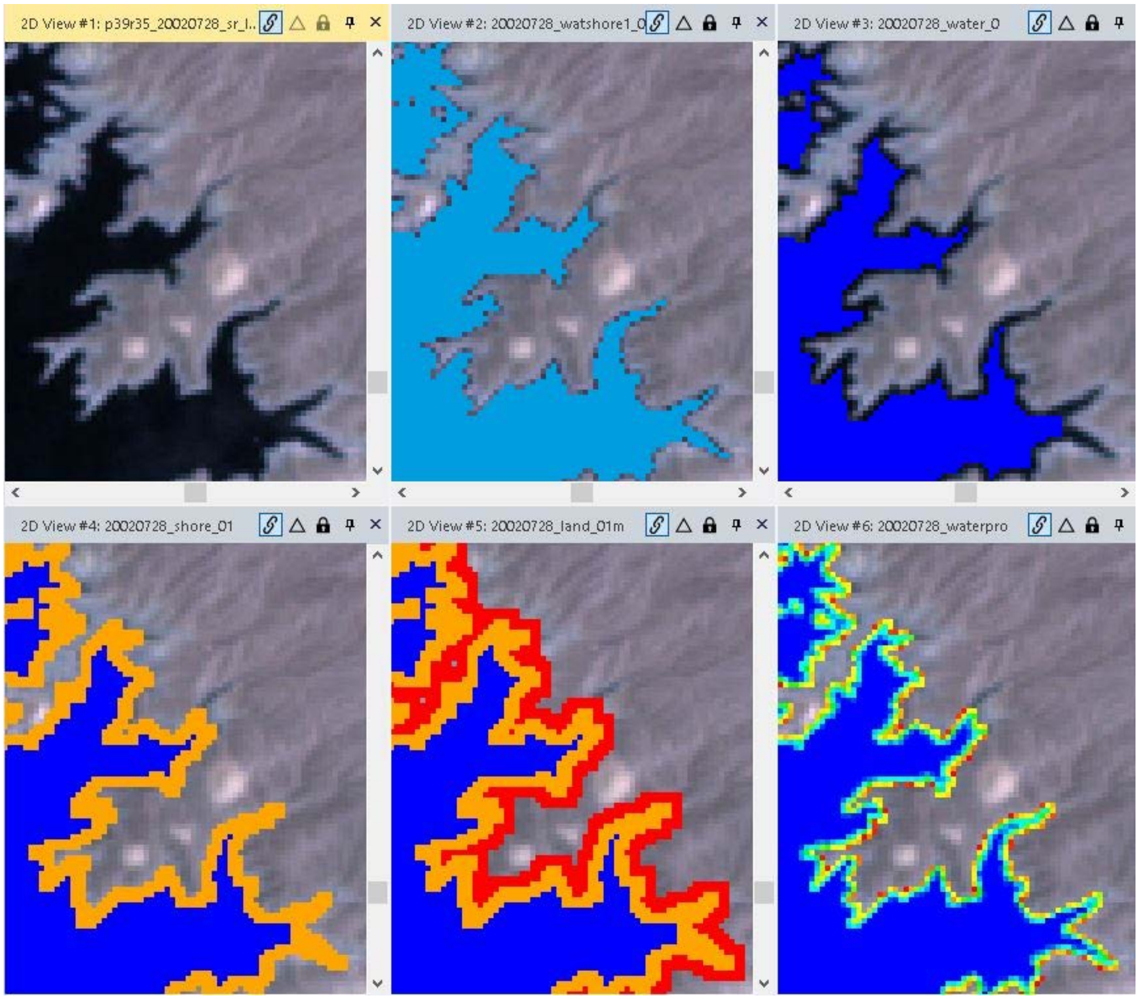

Figure 1. Water proportion mapping procedure. Upper Left: Landsat image of a portion of Lake Mead in Nevada. Upper Center: temp1 mask (light blue) identifying both water and the first ring of shoreline pixels. Upper Right: water_01mask (dark blue) identifying 100% water pixels. Lower Left: water_01mask (dark blue) and shore_01mask (orange) identifying all shoreline pixels for which water proportion will be estimated. Lower Center: water_01mask (dark blue), shore_01mask (orange), and land_01mask (red) identifying land pixels. Lower Right: water proportion image where continuous color ramp indicates water percentage (dark blue: 100%, cyan: 75%, green: 50%, yellow: 25%, red: 1%).

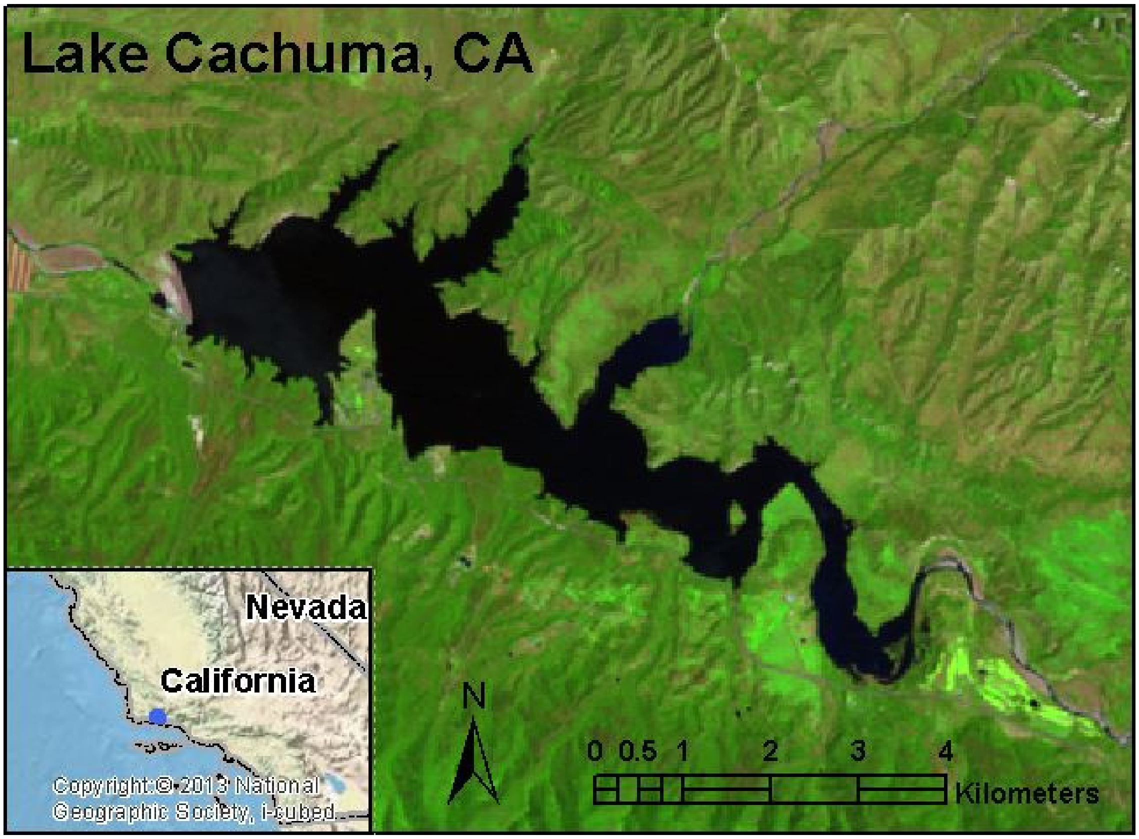

Figure 2. Landsat 5 TM image (SWIR1, NIR, red = RGB) of Lake Cachuma, California, acquired on 4/29/2011.

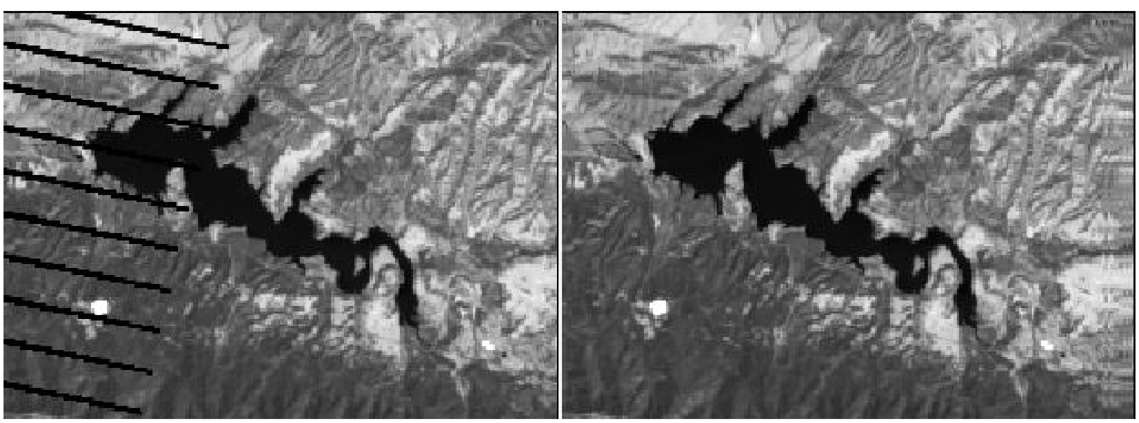

Figure 3. Landsat 7 ETM+ image of Lake Cachuma, California acquired on 7/28/2012 before (left) and after (right) the data-gap filling procedure.

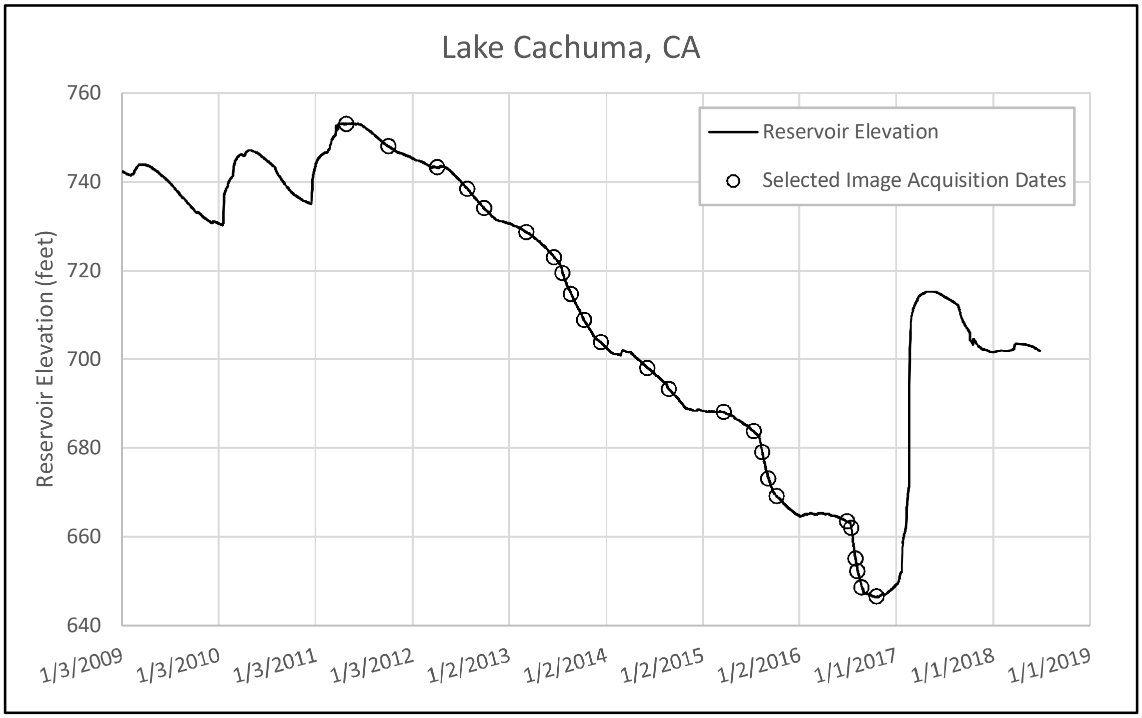

Figure 4. Reservoir elevations and image acquisition dates for Lake Cachuma, California.

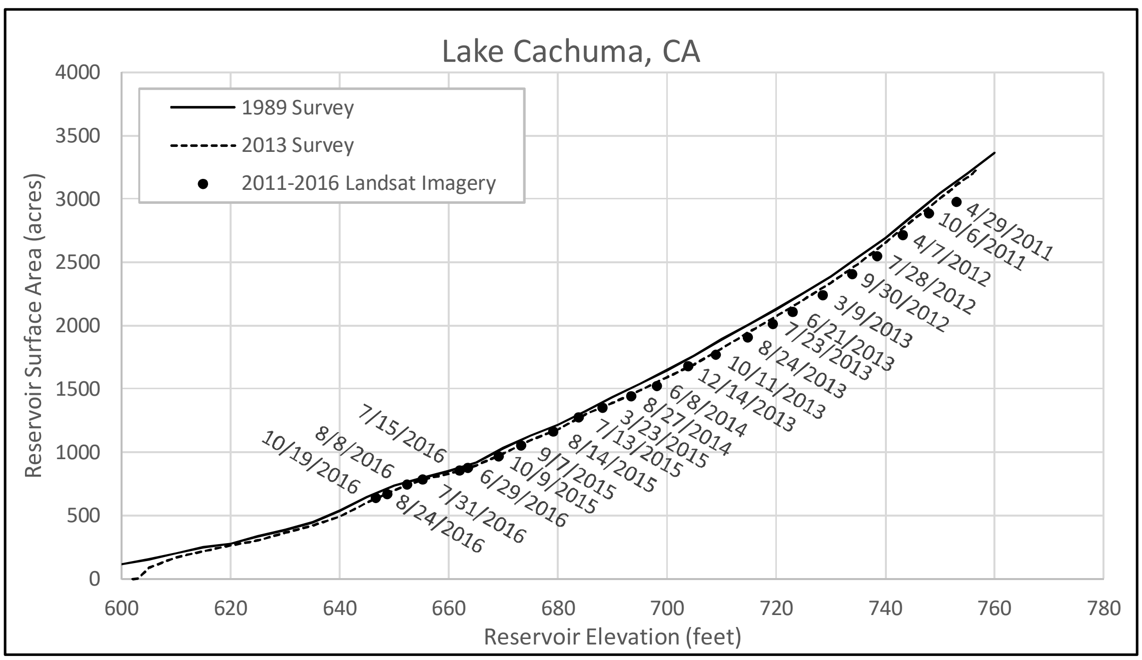

Figure 5. Lake Cachuma surface areas calculated from reservoir survey data, Landsat imagery, and high-resolution imagery.

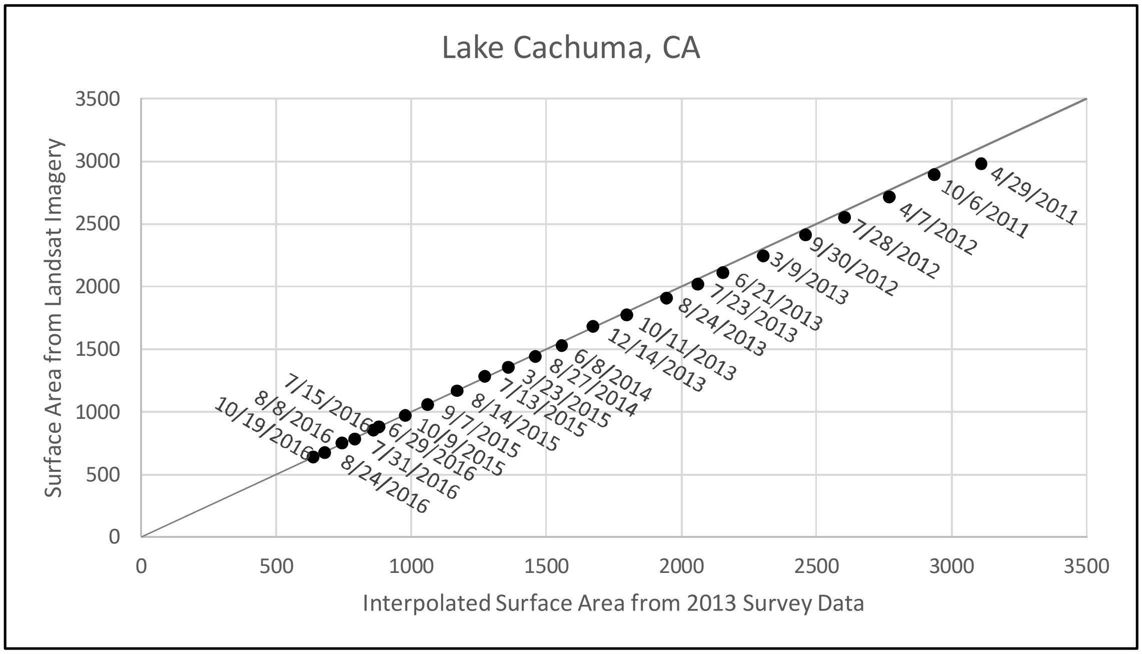

Figure 6. Comparison of Lake Cachuma surface area estimates generated from 2013 survey data and 2011-2016 Landsat imagery.

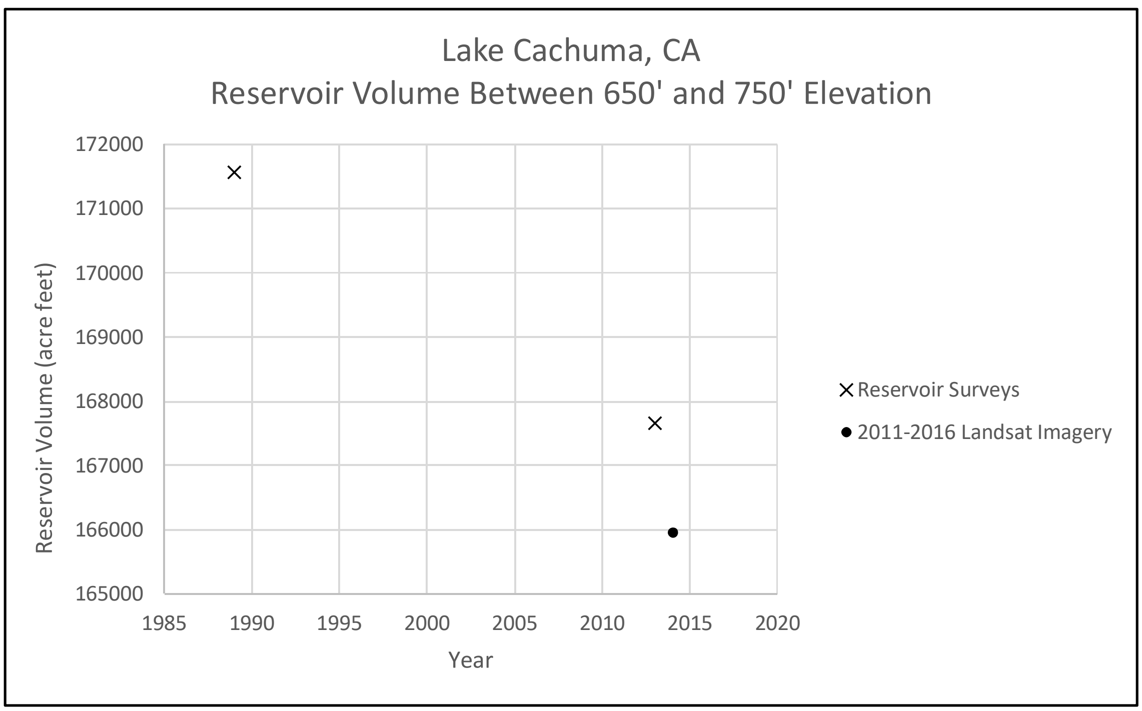

Figure 7. Lake Cachuma Reservoir volume estimates between 650 and 750 feet reservoir elevation.

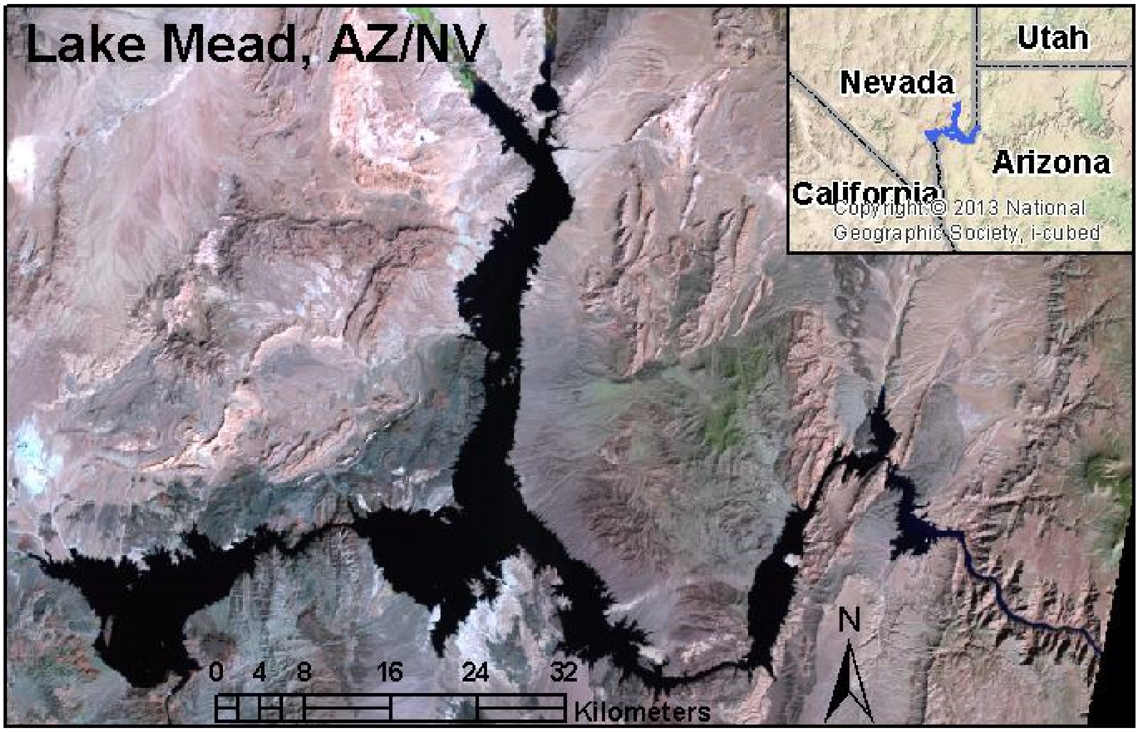

Figure 8. Landsat 5 TM image (SWIR1, NIR, red = RGB) of Lake Mead, Arizona/Nevada acquired on 3/16/2000.

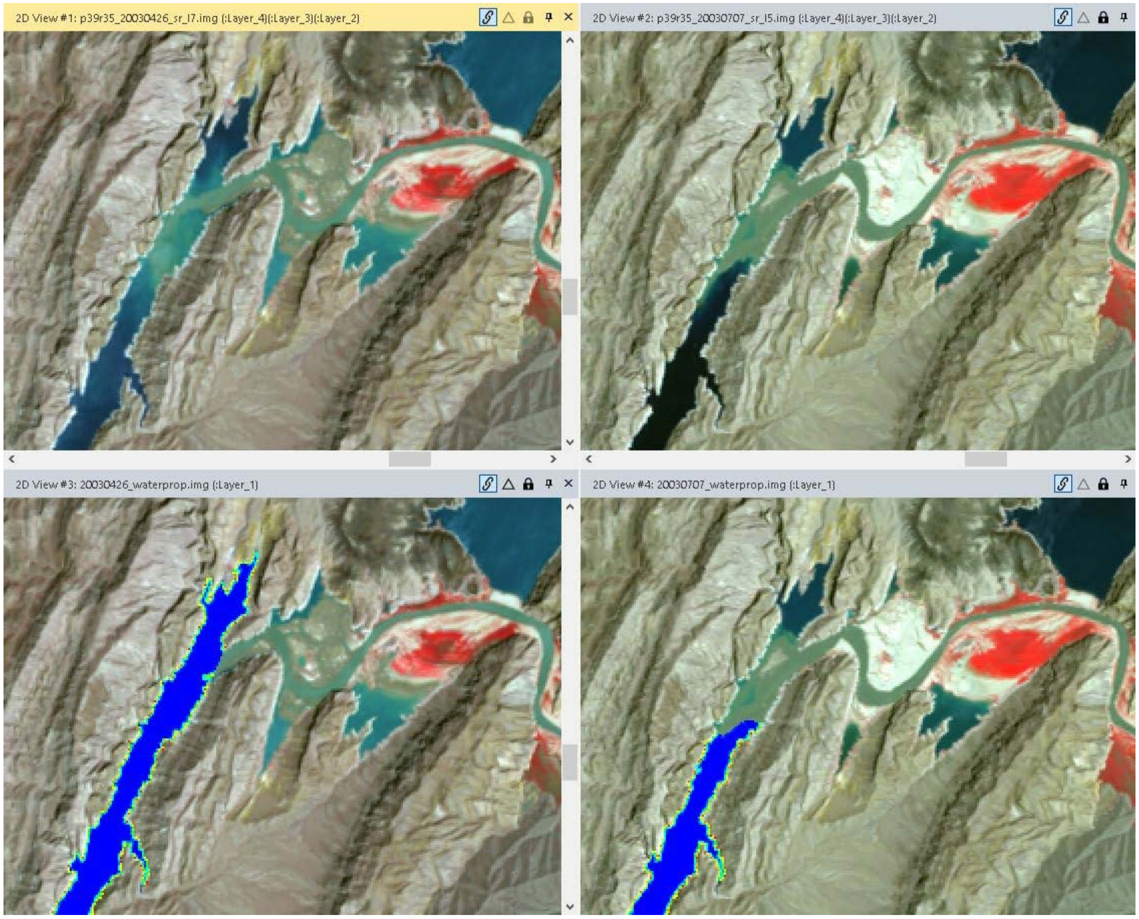

Figure 9. Landsat images (NIR, red, green = R, G, B) acquired on 4/26/2003 at reservoir elevation 1149.01' (left) and on 7/7/2003 at reservoir elevation 1143.04; (right). Top panels contain images only, while bottom panels show the Landsat images overlain by color-coded water proportion images (blue = 100% → red = 1%).

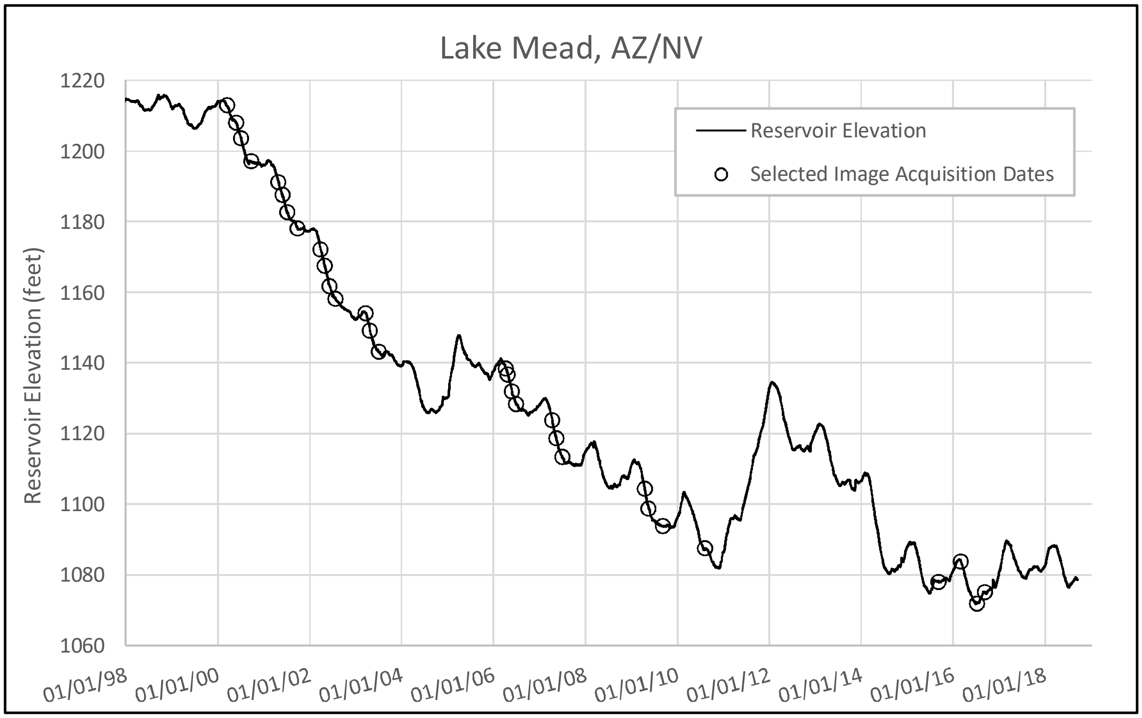

Figure 10. Reservoir elevations and image acquisition dates for Lake Mead, Arizona/Nevada.

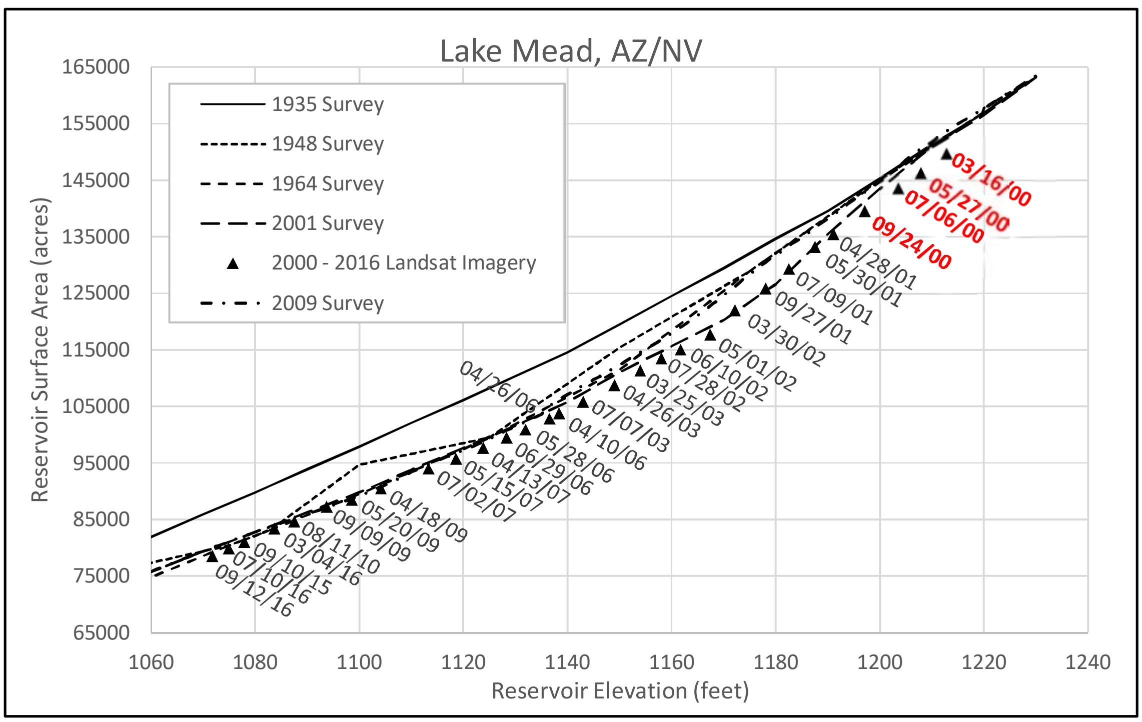

Figure 11. Lake Mead surface areas calculated from reservoir survey data and Landsat imagery.

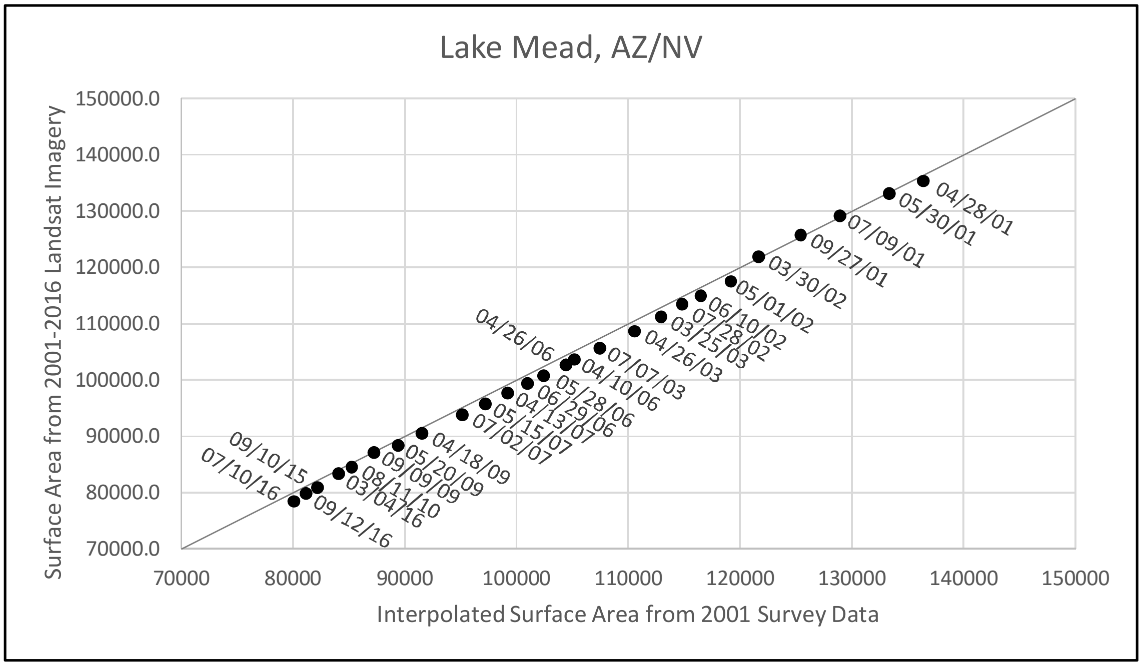

Figure 12. Comparison of Lake Mead surface area estimates generated from 2001 survey data and 2001 - 2016 Landsat imagery. RSA data from the four images whose reservoir boundary was clipped at the Grand Wash Cliffs are not included in this Figure.

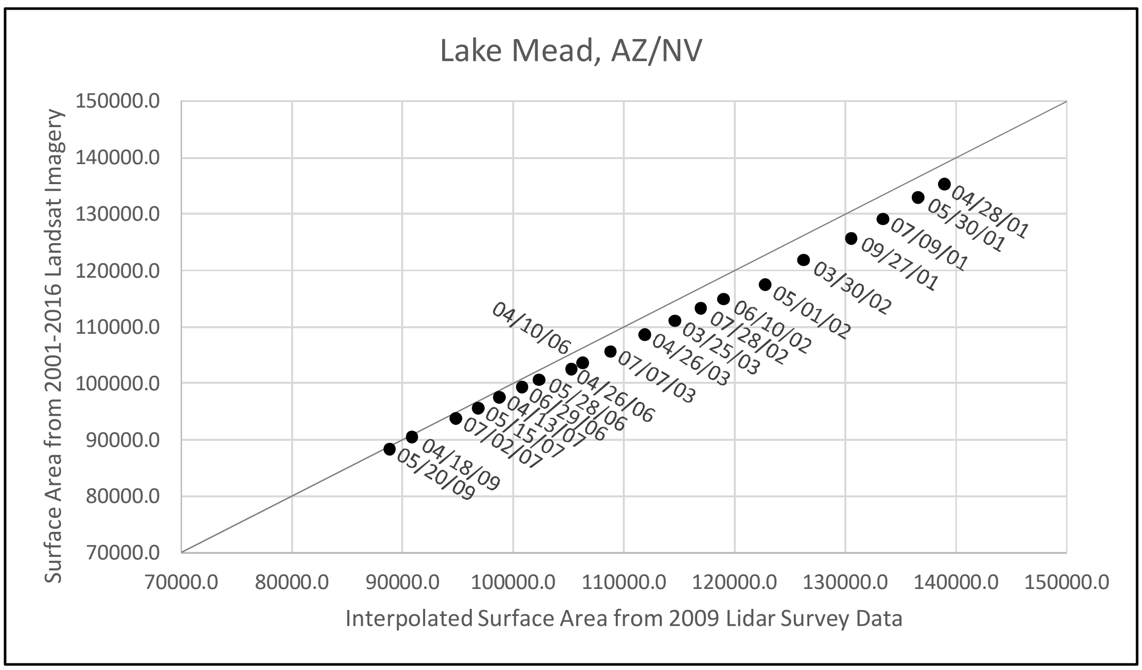

Figure 13. Comparison of Lake Mead surface area estimates generated from 2009 lidar survey data and 2001 - 2016 Landsat imagery. RSA data from the four images whose reservoir boundary was clipped at the Grand Wash Cliffs are not included in this Figure.

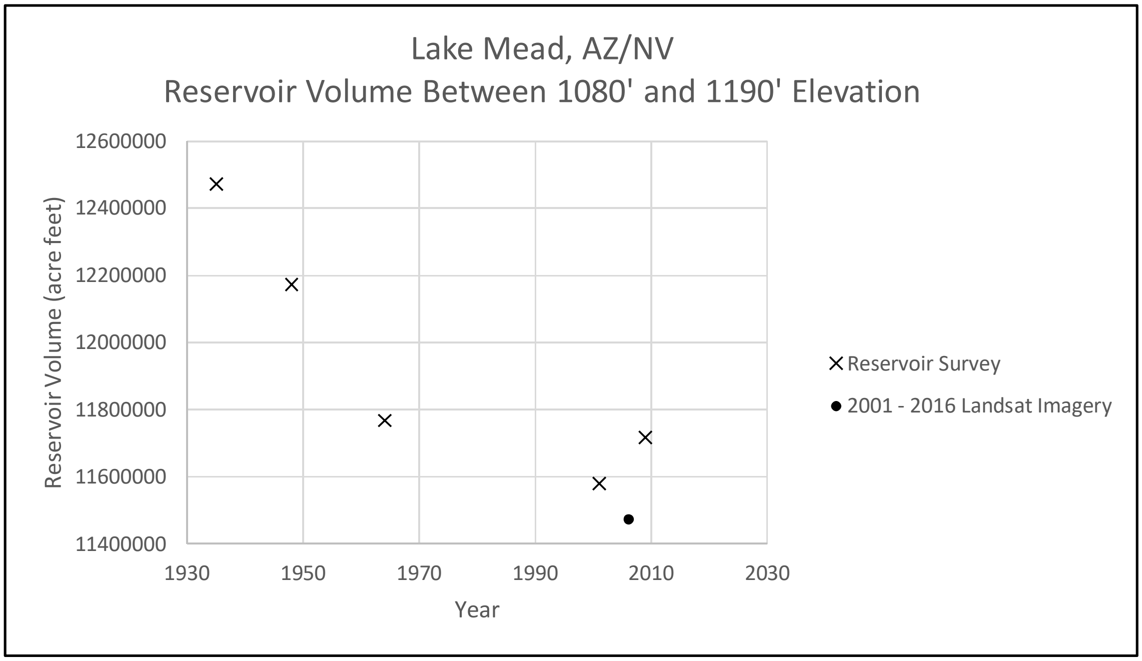

Figure 14. Lake Mead volume estimates between 1080 and 1190 feet reservoir elevation.

Figure 15. Landsat 5 TM image (SWIR1, NIR, red = RGB) of Elephant Butte Reservoir, New Mexico acquired on 6/29/1998.

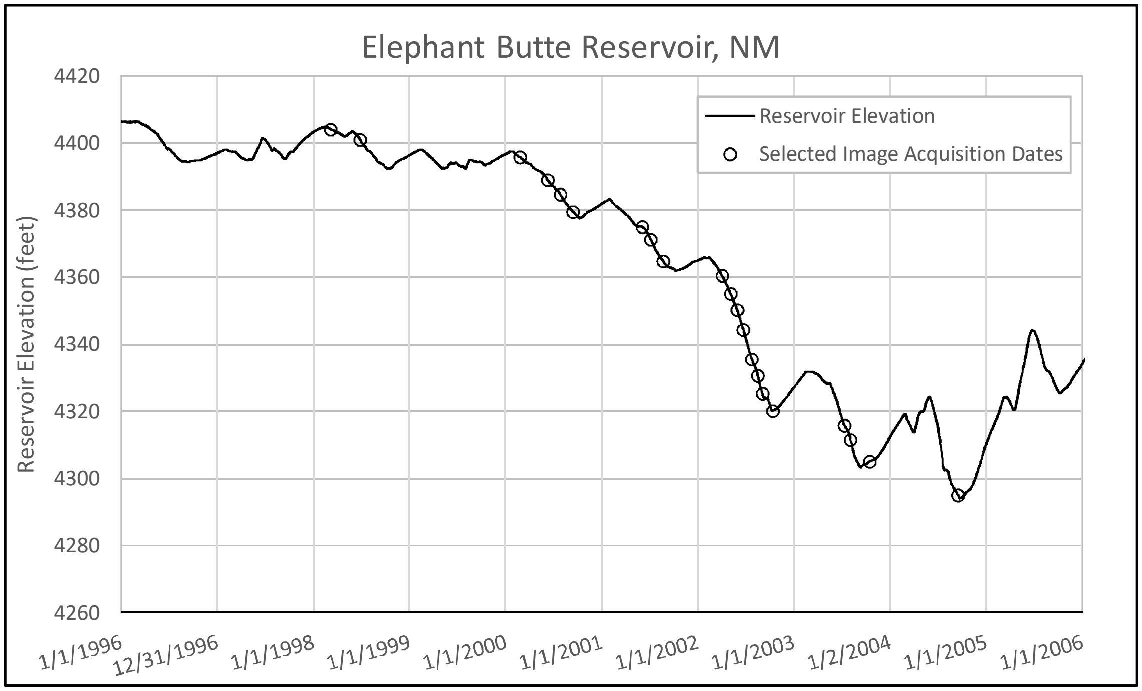

Figure 16. Reservoir elevations and image acquisition dates for Elephant Butte Reservoir, New Mexico.

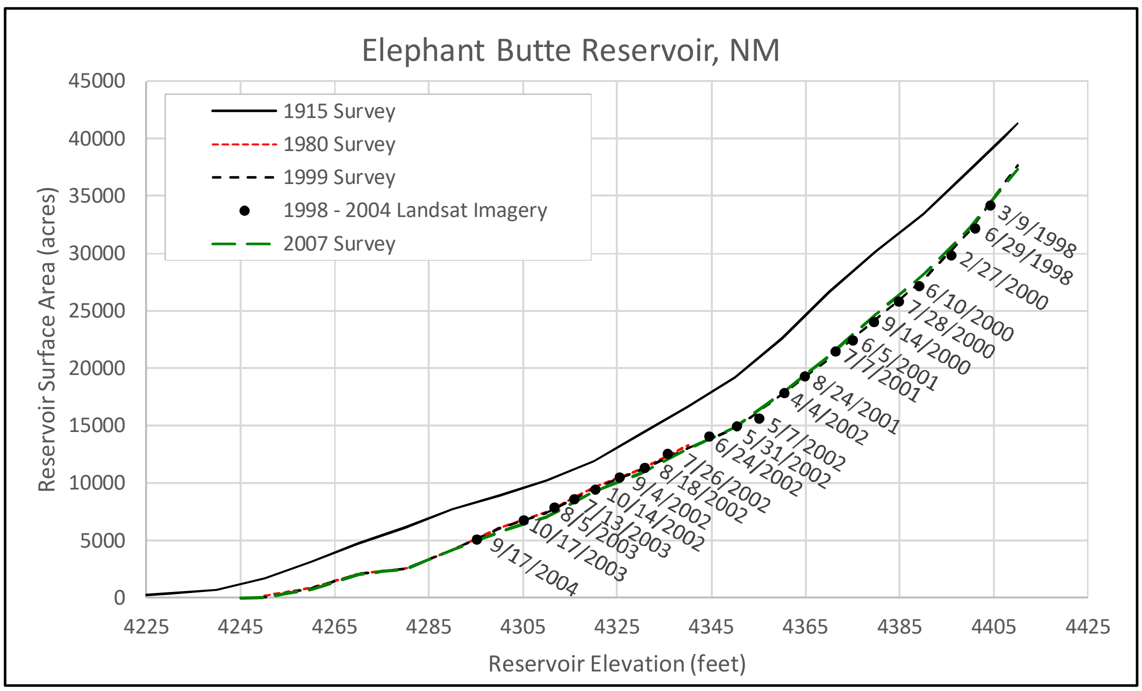

Figure 17. Elephant Butte Reservoir surface areas calculated from reservoir survey data and Landsat imagery.

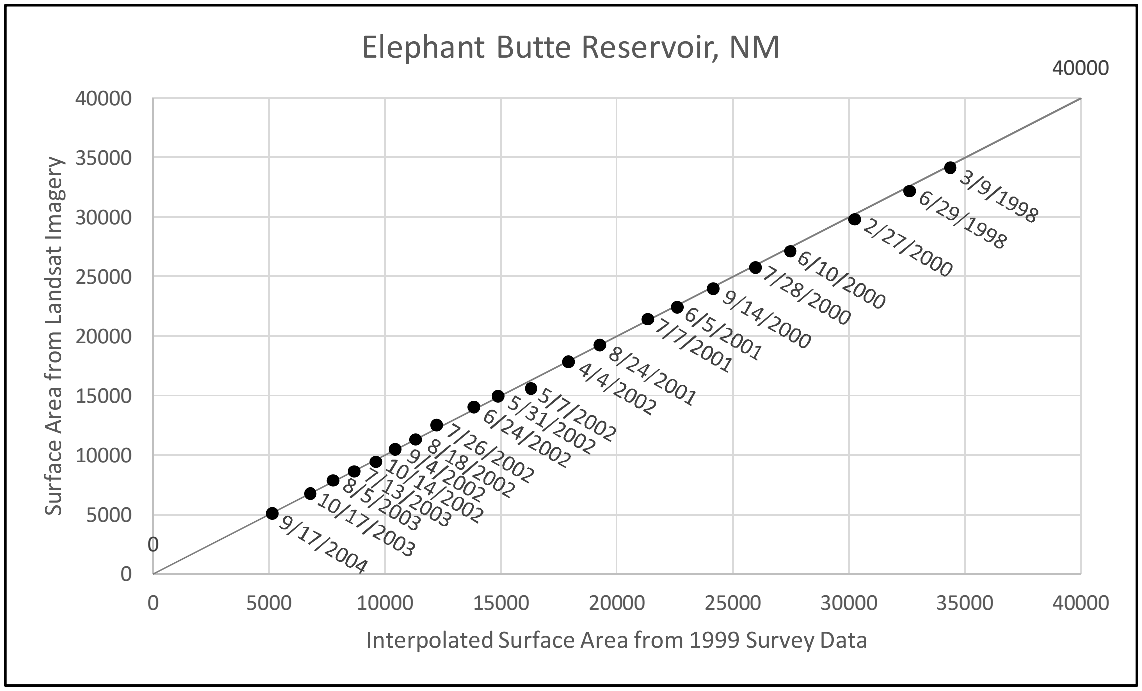

Figure 18. Comparison of Elephant Butte Reservoir surface area estimates generated from 1999 survey data and 1998 - 2004 Landsat imagery.

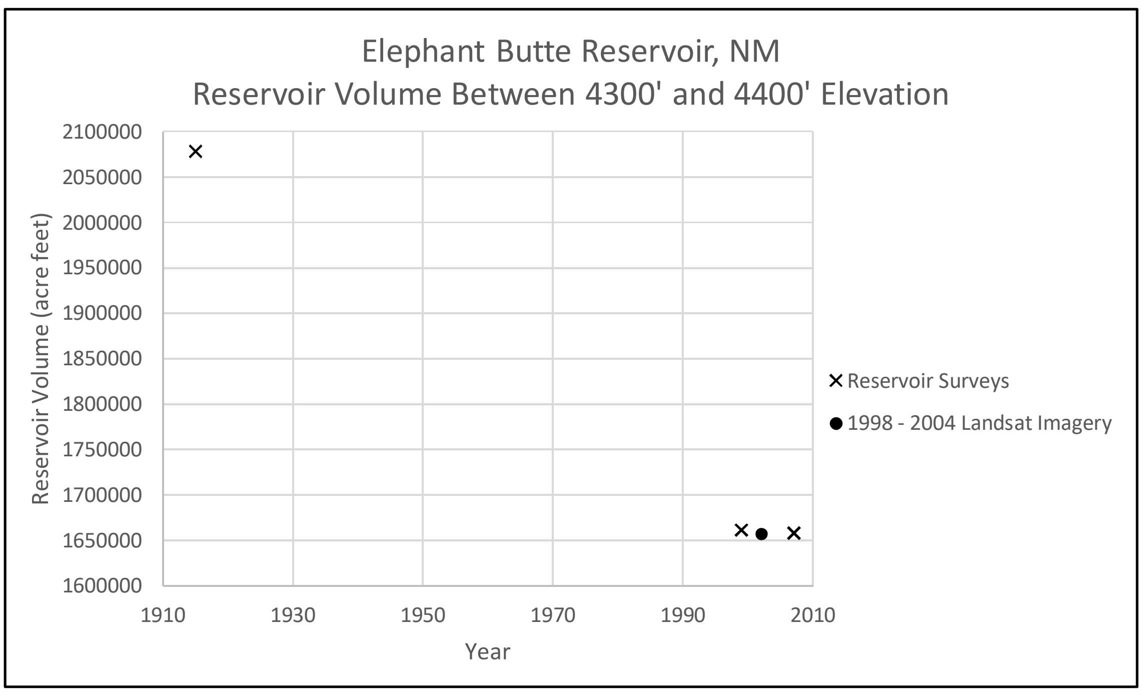

Figure 19. Elephant Butte Reservoir volume estimates between 4300 and 4400 feet reservoir elevation.

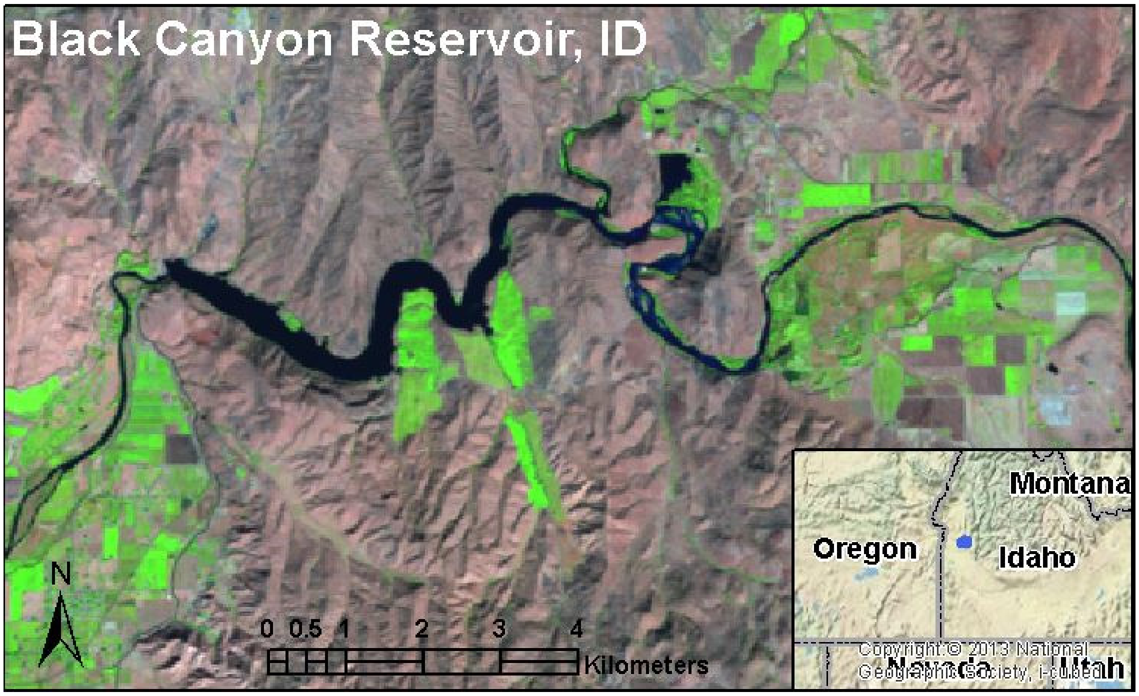

Figure 20. Landsat 5 TM image (SWIR1, NIR, red = RGB) of Black Canyon Reservoir, Idaho acquired on 10/6/2002.

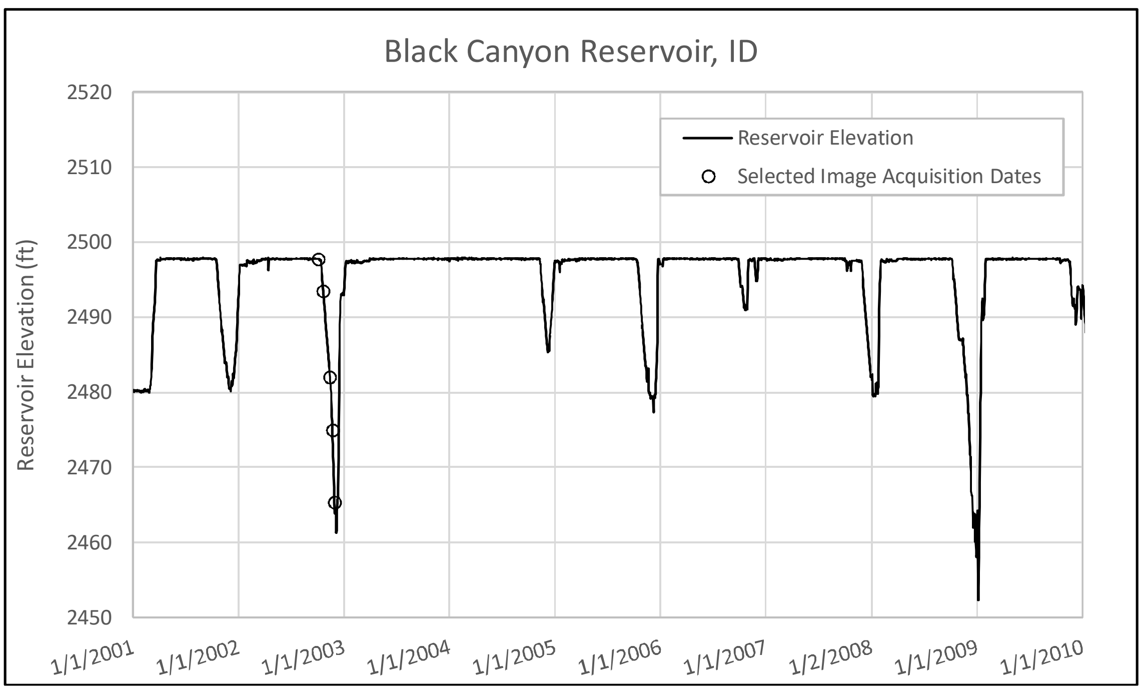

Figure 21. Reservoir elevations and image acquisition dates for Black Canyon Reservoir, Idaho.

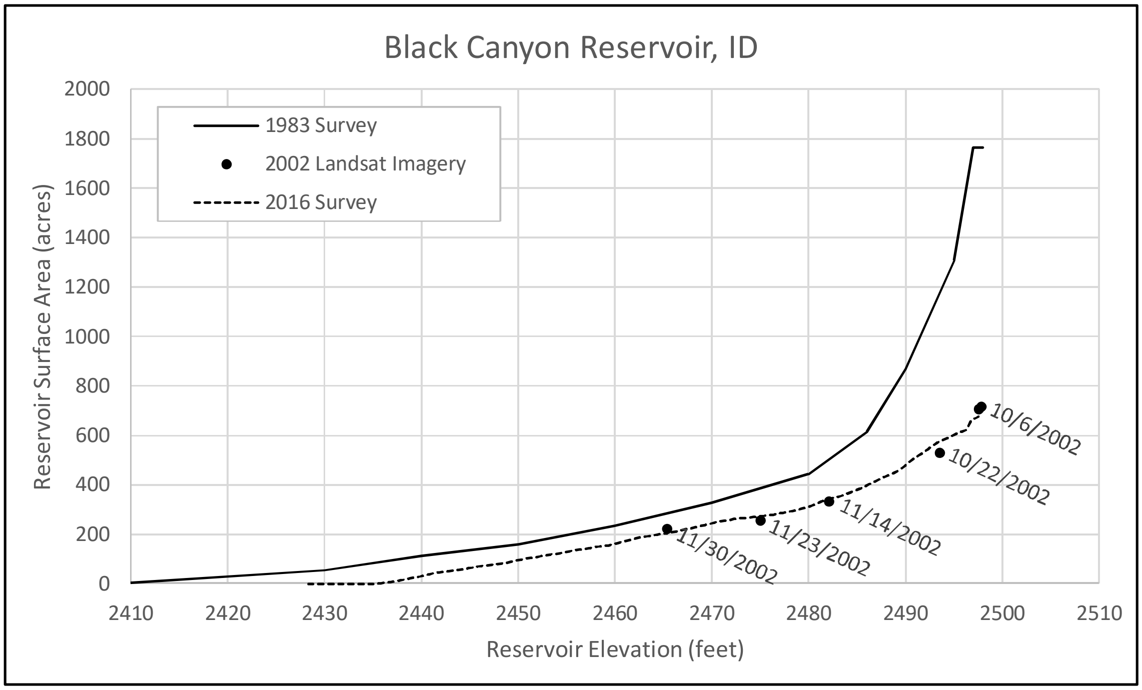

Figure 22. Black Canyon Reservoir surface areas calculated from reservoir survey data and Landsat imagery.

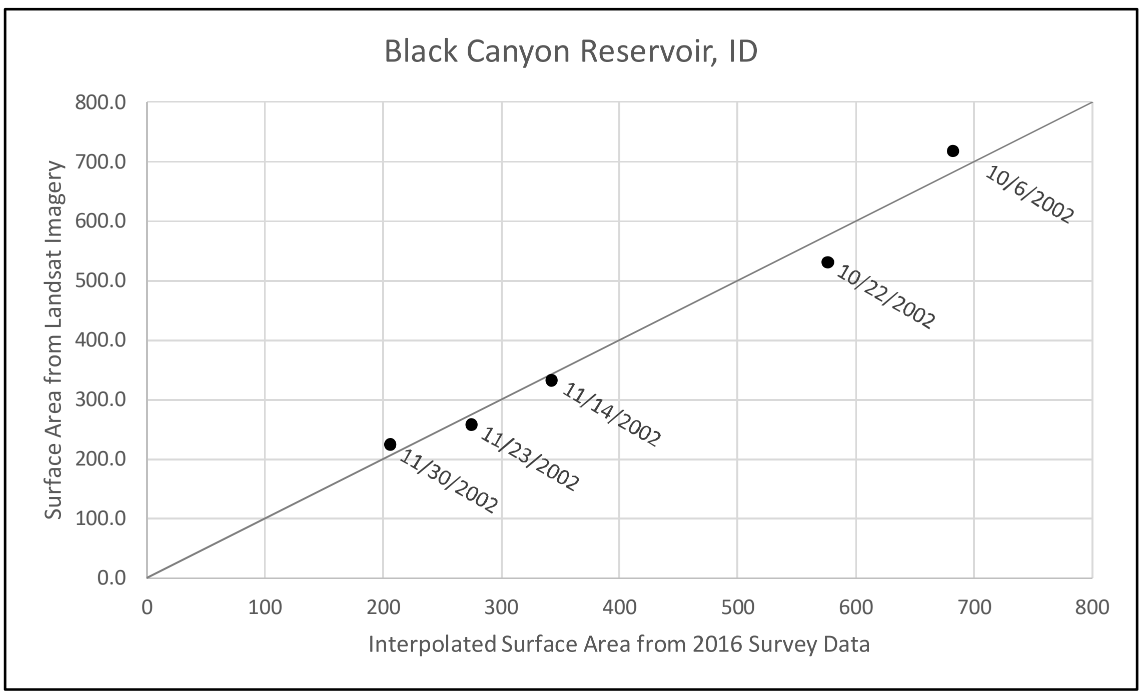

Figure 23. Comparison of Black Canyon Reservoir surface area estimates generated from 2016 survey data and 2002 Landsat imagery.

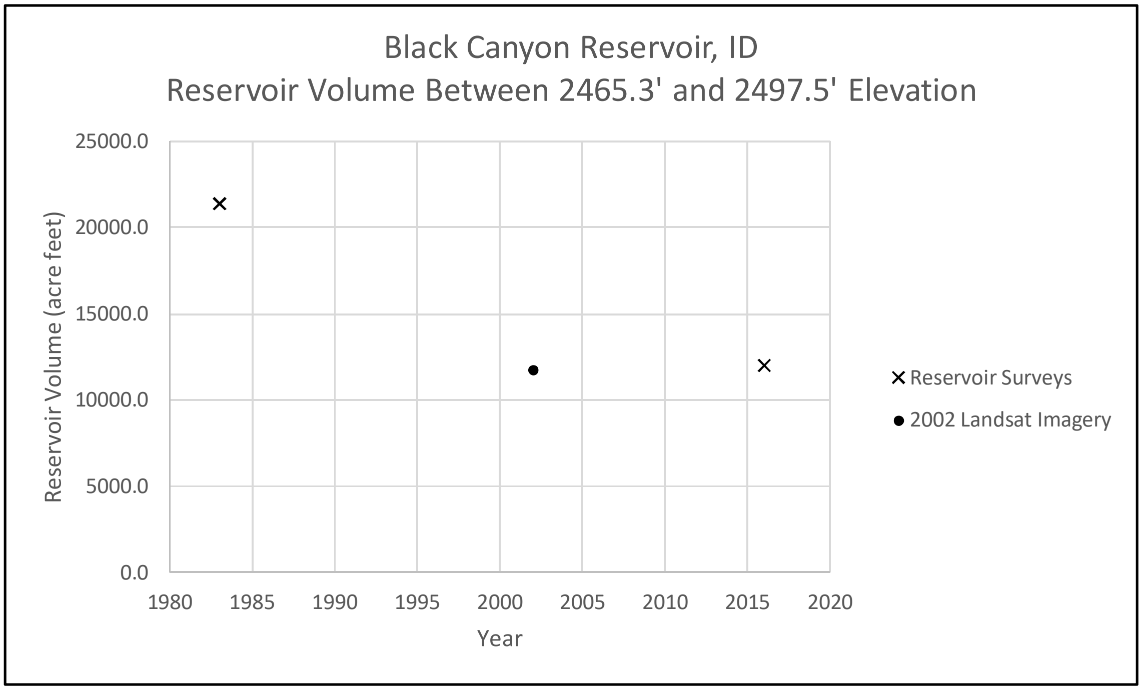

Figure 24. Black Canyon Reservoir volume estimates between 2465.3 and 2497.5 feet reservoir elevation.

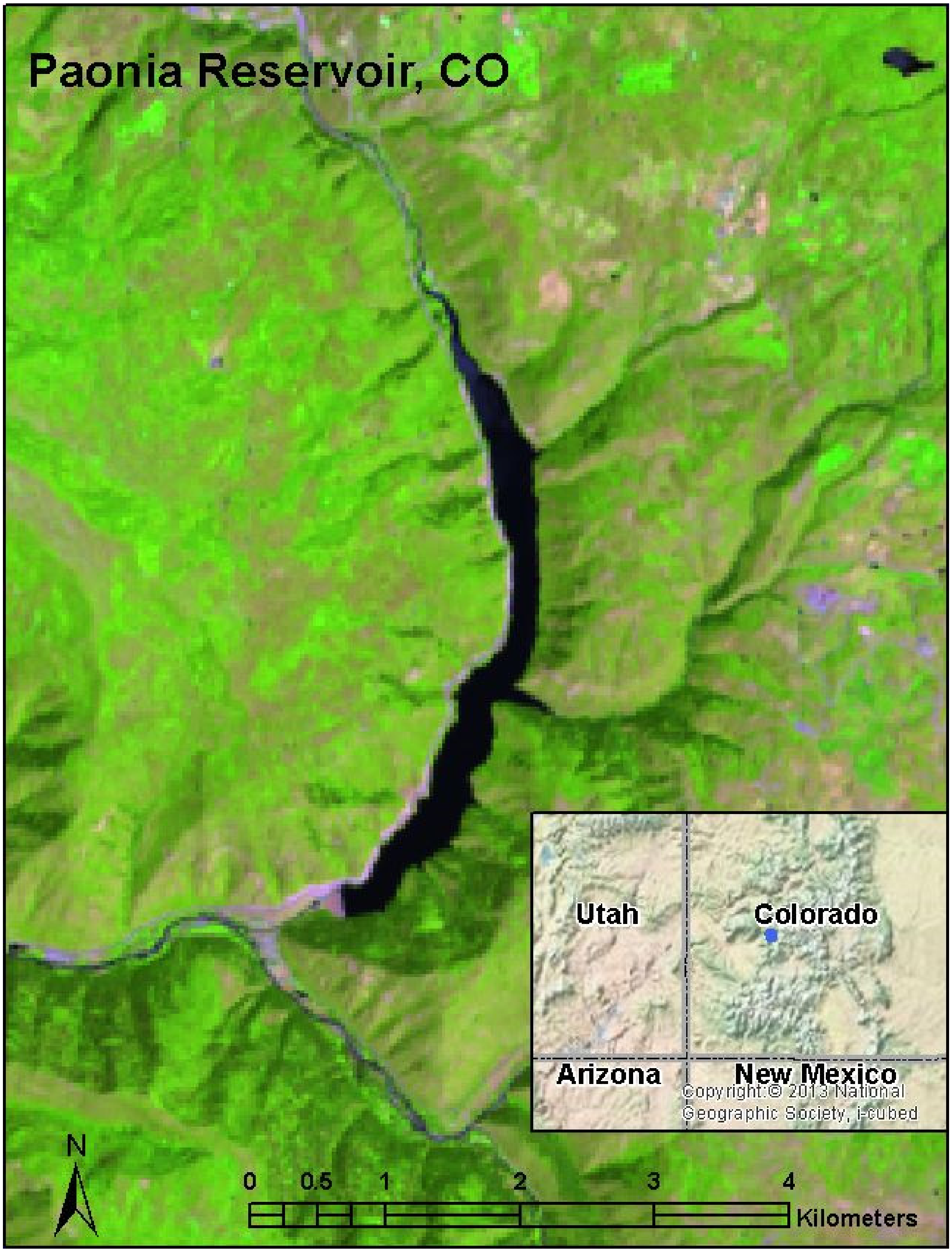

Figure 25. Landsat 7 ETM+ image (SWIR1, NIR, red = RGB) of Paonia Reservoir, Colorado acquired on 7/1/2017.

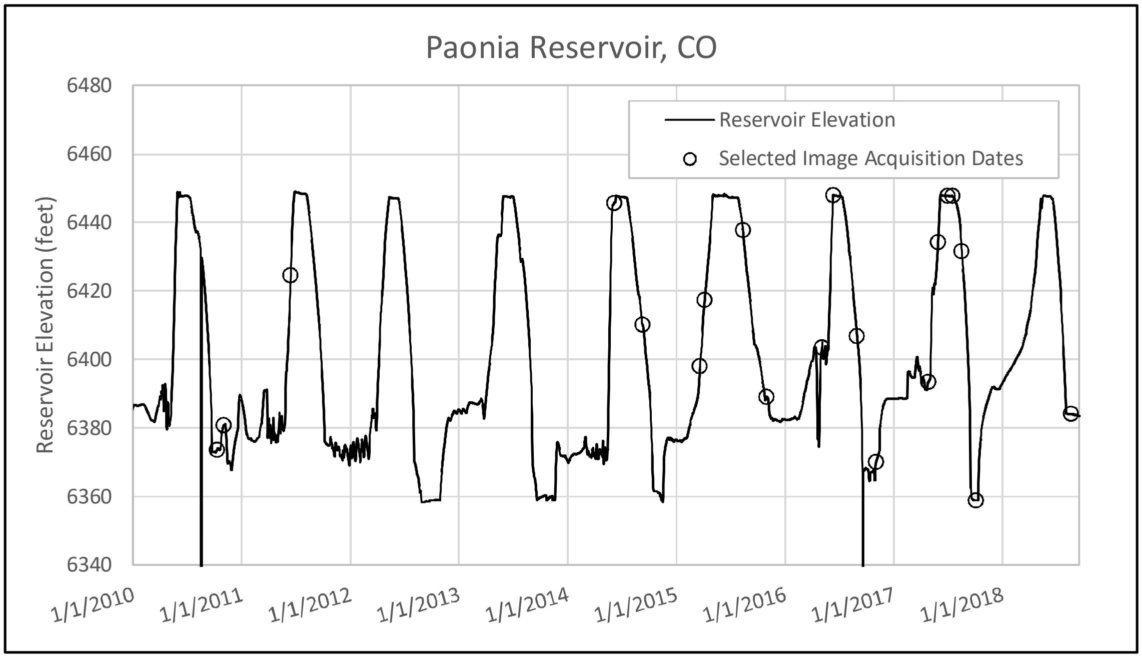

Figure 26. Reservoir elevations and image acquisition dates for Paonia Reservoir, Colorado.

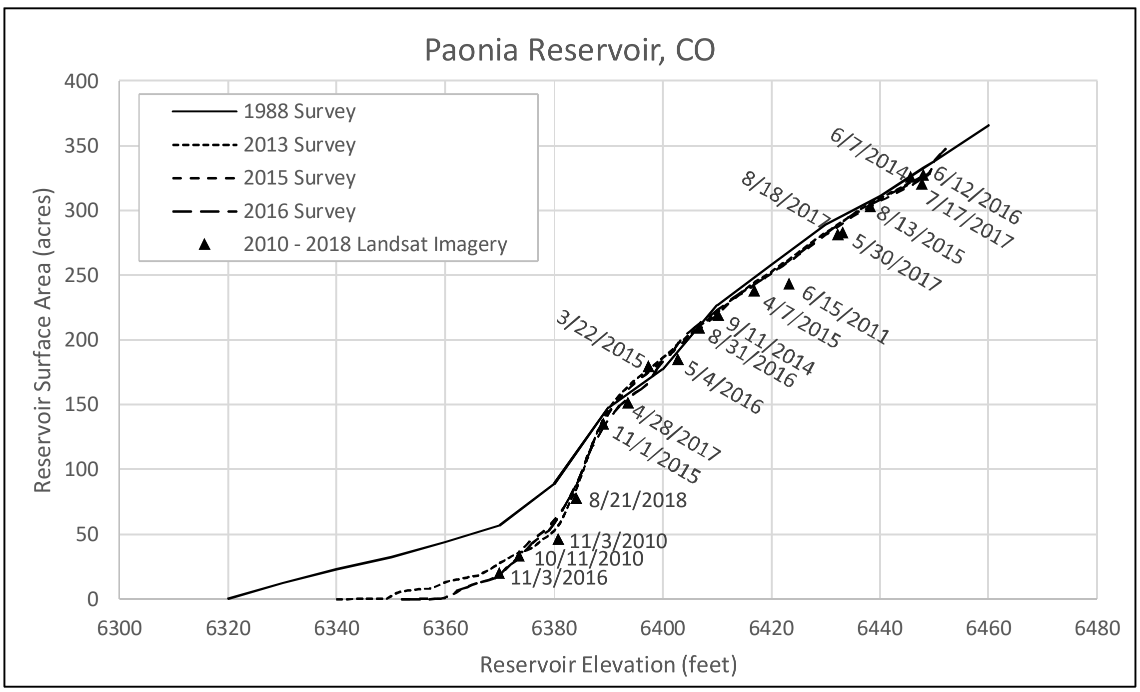

Figure 27. Paonia Reservoir surface areas calculated from reservoir survey data and Landsat imagery.

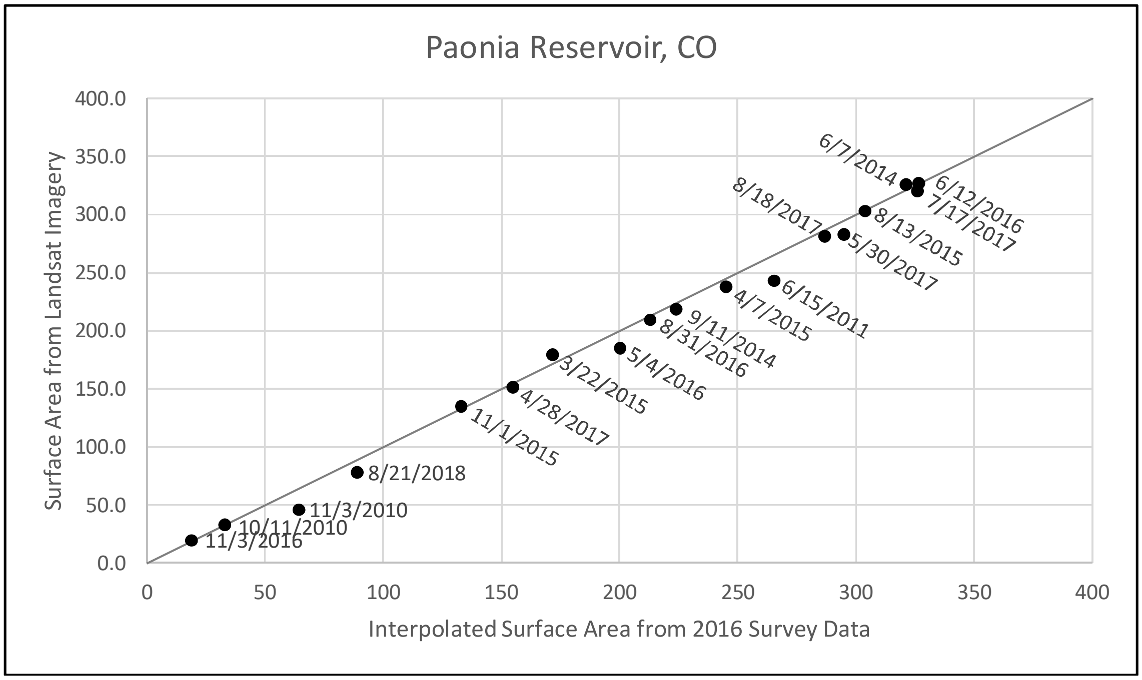

Figure 28. Comparison of Paonia Reservoir surface area estimates generated from 2016 survey data and 2010 - 2018 Landsat imagery.

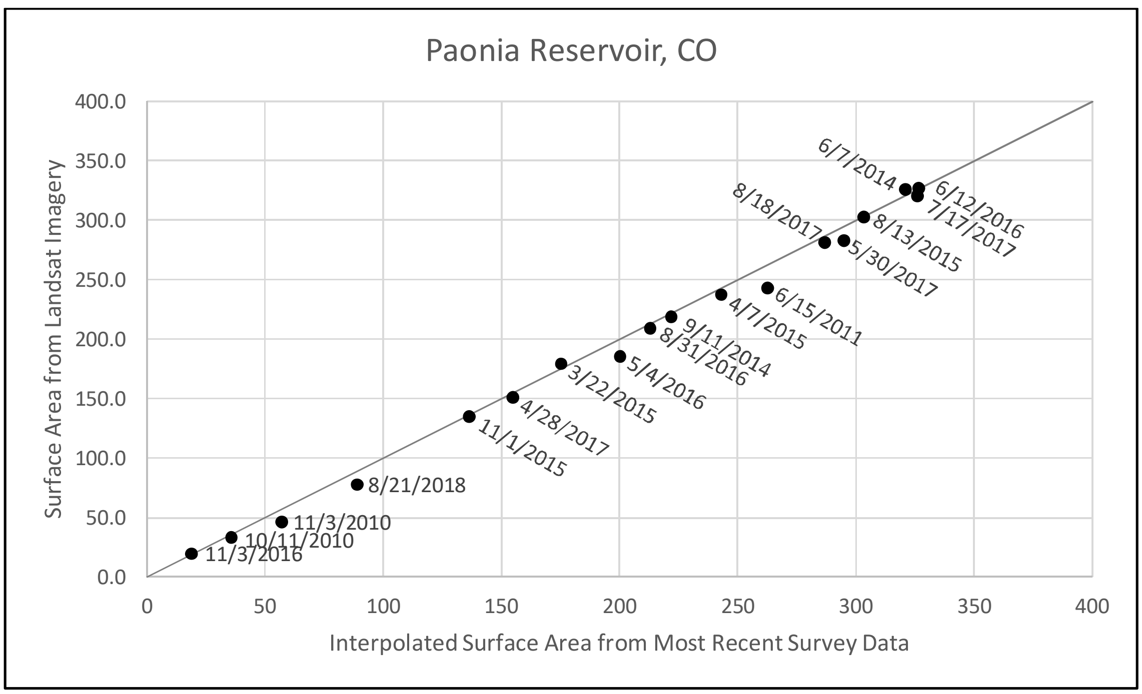

Figure 29. Comparison of Paonia Reservoir surface area estimates generated from 2013, 2015, and 2016 survey data and 2010 - 2018 Landsat imagery.

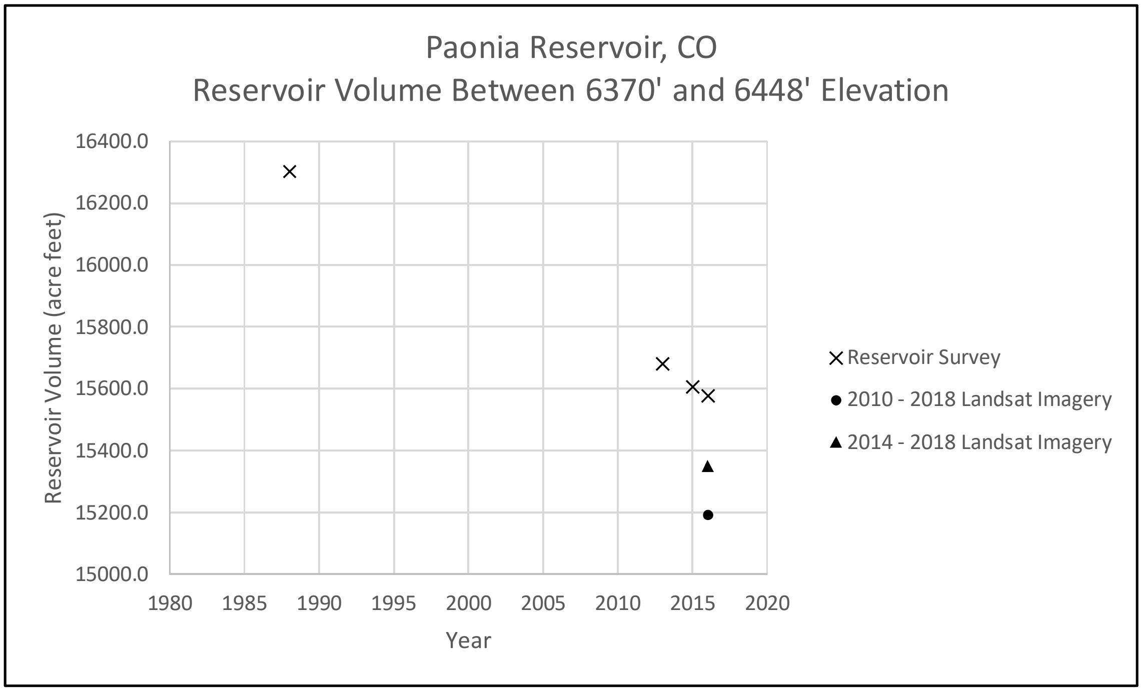

Figure 30. Paonia Reservoir volume estimates between 6370 and 6448 feet reservoir elevation.

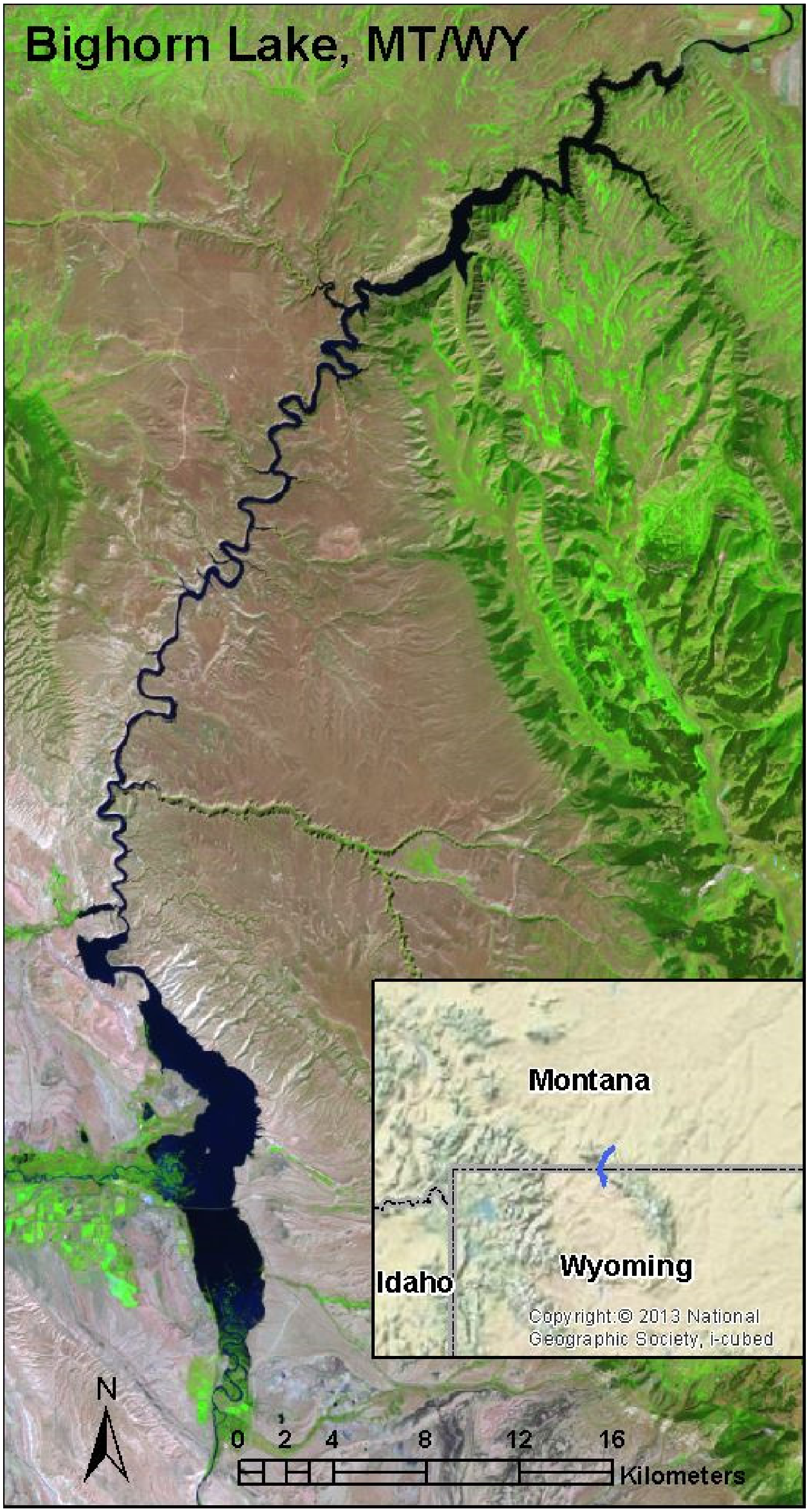

Figure 31. Landsat 5 TM image (SWIR1, NIR, red = RGB) of Bighorn Lake, Montana/Wyoming acquired on 7/24/2011.

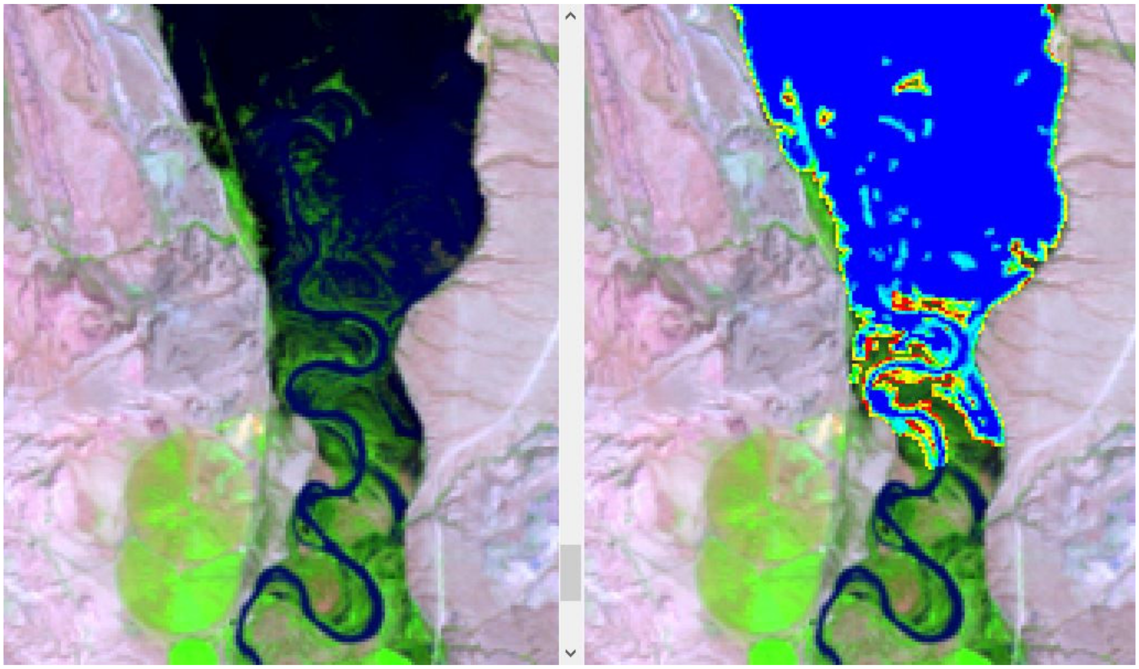

Figure 32. 7/24/2011 Landsat 8 image (SWIR1, NIR, red = R, G, B) of the inflow of the Bighorn River into Bighorn Lake. The left pane shows only the image, and the right contains the image overlain by the color-coded water proportion image for that date (blue = 100% water → red = 1% water).

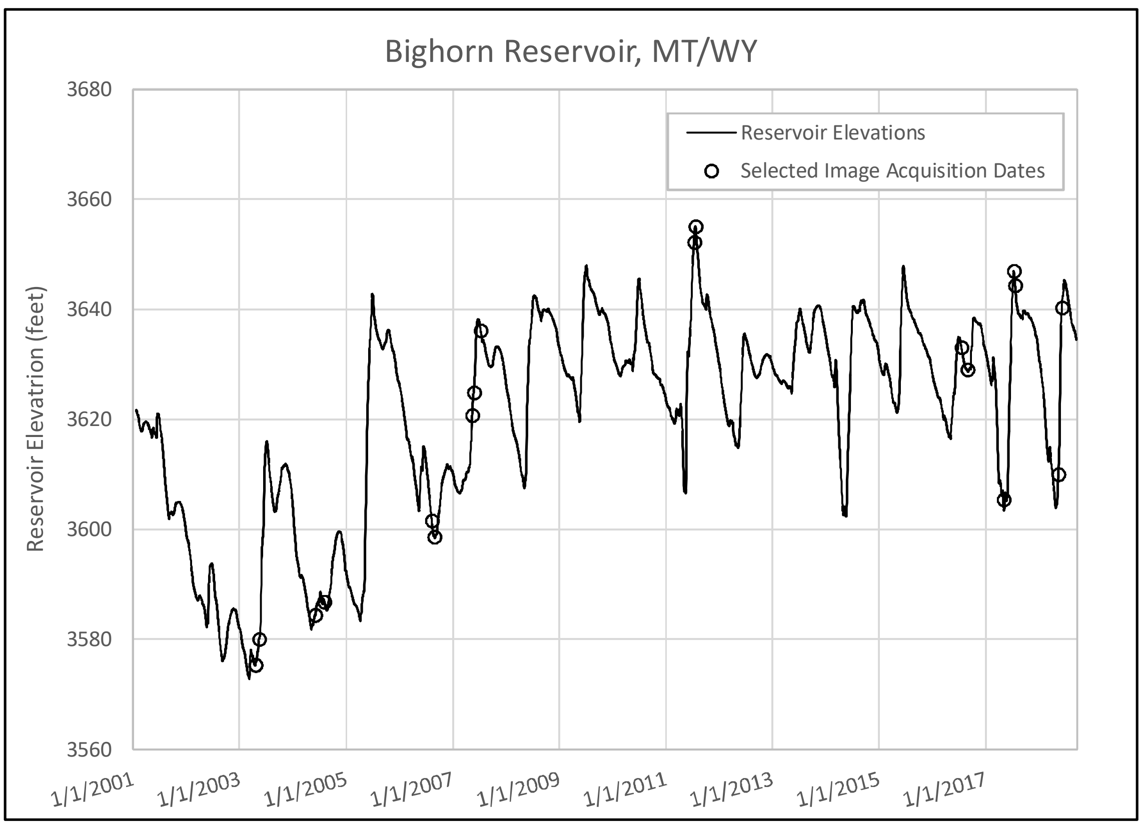

Figure 33. Reservoir elevations and image acquisition dates for Bighorn Lake, Montana/Wyoming.

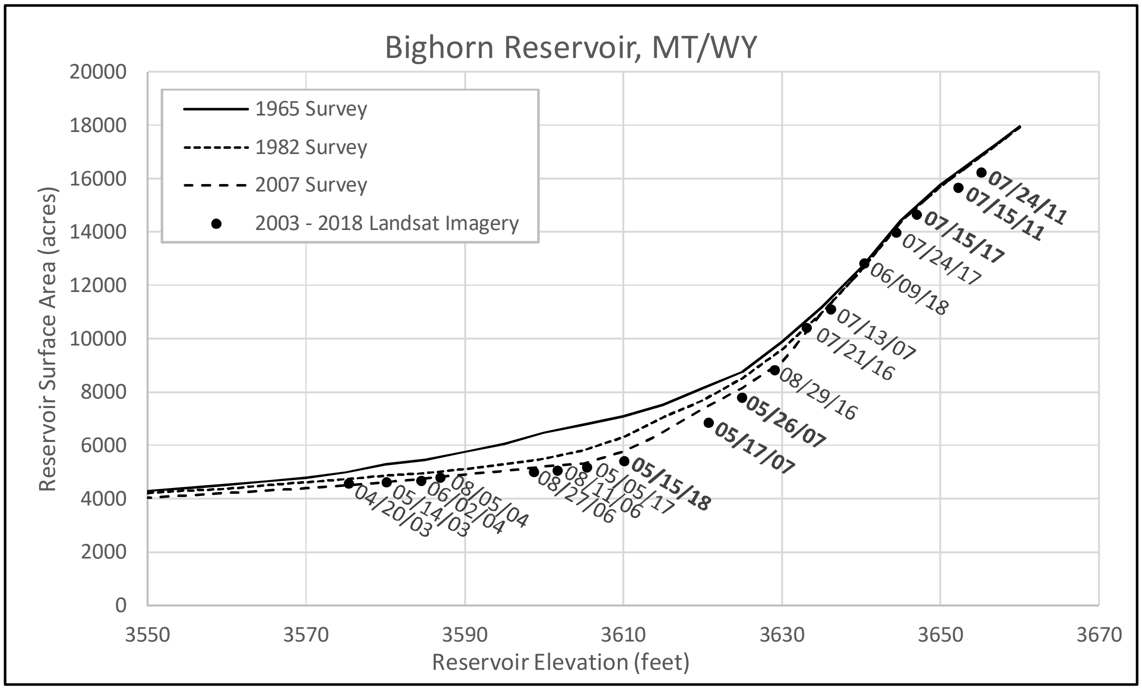

Figure 34. Bighorn Lake surface areas calculated from reservoir survey data and Landsat imagery.

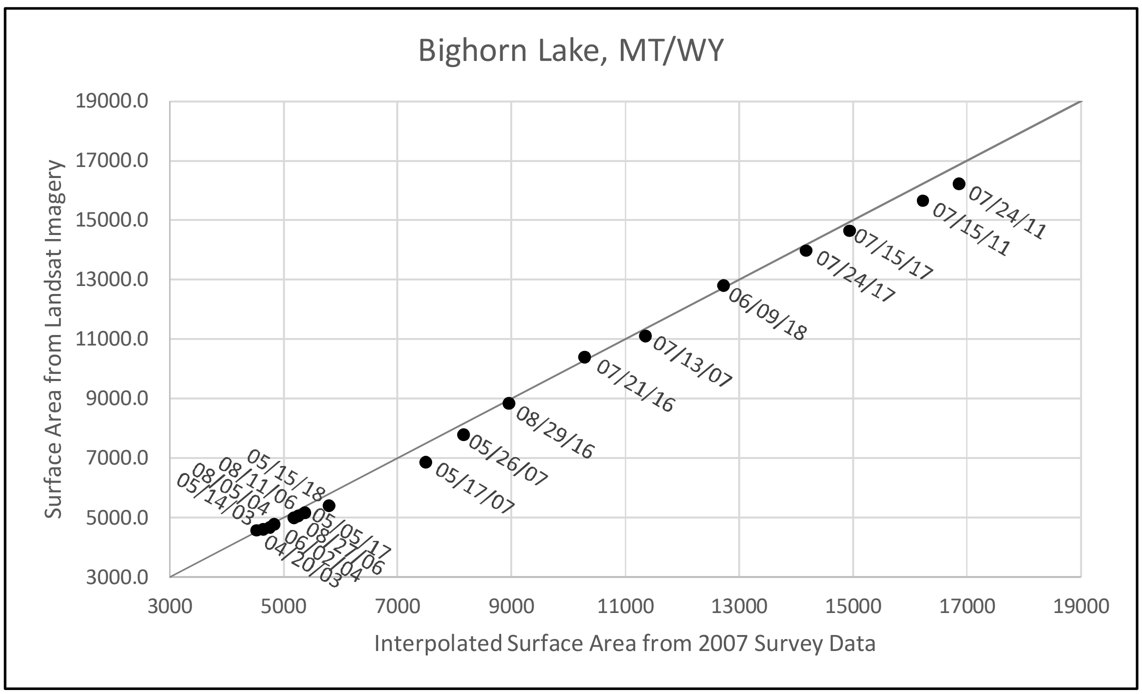

Figure 35. Comparison of Bighorn Lake surface area estimates generated from 2007 survey data and 2003 - 2018 Landsat imagery.

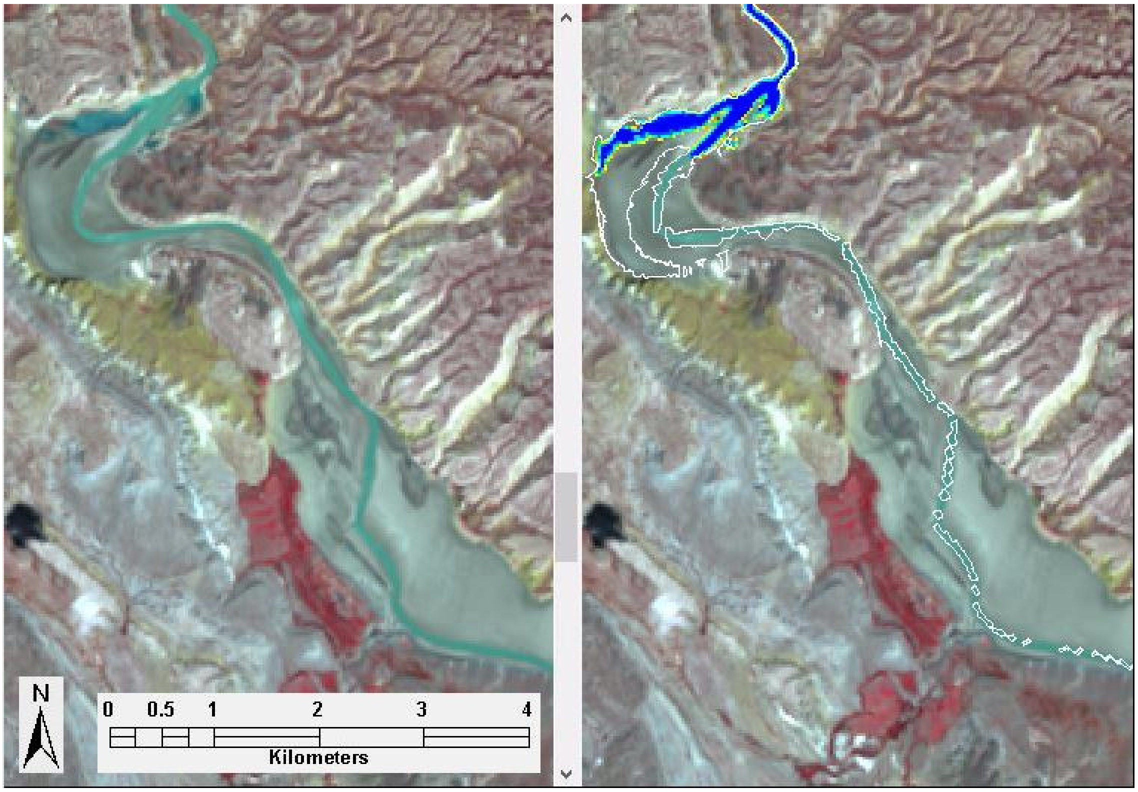

Figure 36. Landsat 8 OLI image of the inflow of the Bighorn River into Bighorn Lake on 5/15/2018. Left panel contains the image only (NIR, red, green = RGB) ; right panel contains the image, color-coded water surface area map generated from Landsat imagery (at reservoir elevation of 3610.04 feet), and 3610-foot contour from the 2007 survey. The 2007 survey identifies ~300 acres that is above the reservoir pool, about evenly distributed between river channel and open ground above the reservoir.

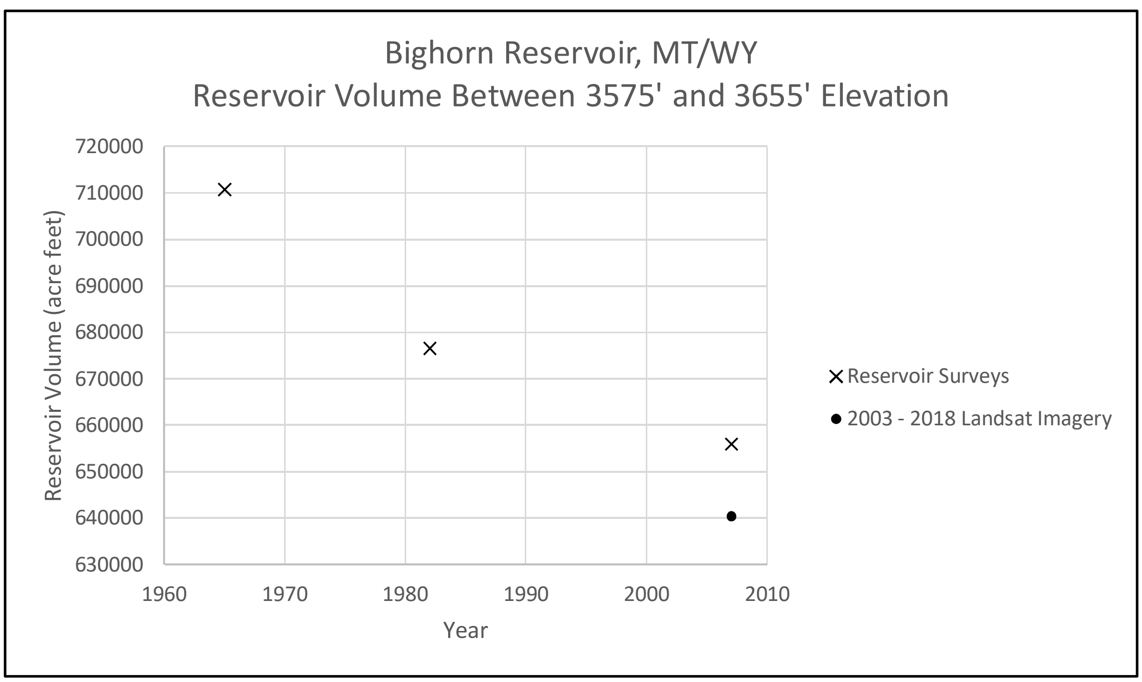

Figure 37. Bighorn Lake volume estimates between 3575 and 3655 feet reservoir elevation.

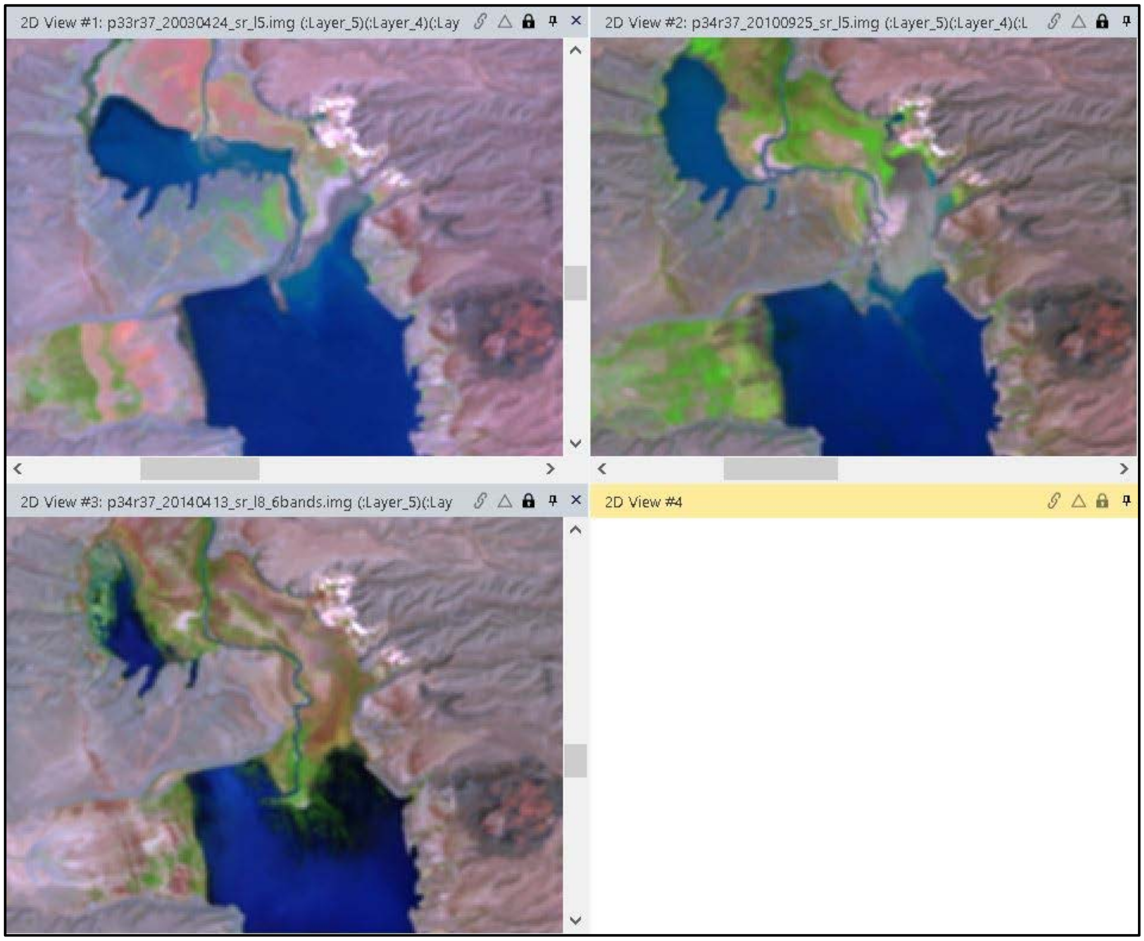

Figure 38. Rio Grande River inflow to Elephant Butte Reservoir at reservoir elevation ≈ 4329.1 feet.
Upper Left: 4/24/2003 (elev = 4329.12'), Upper Right: 9/25/2010 (elev = 4329.13'),
Lower Left: 4/13/2014 (elev = 4329.14')

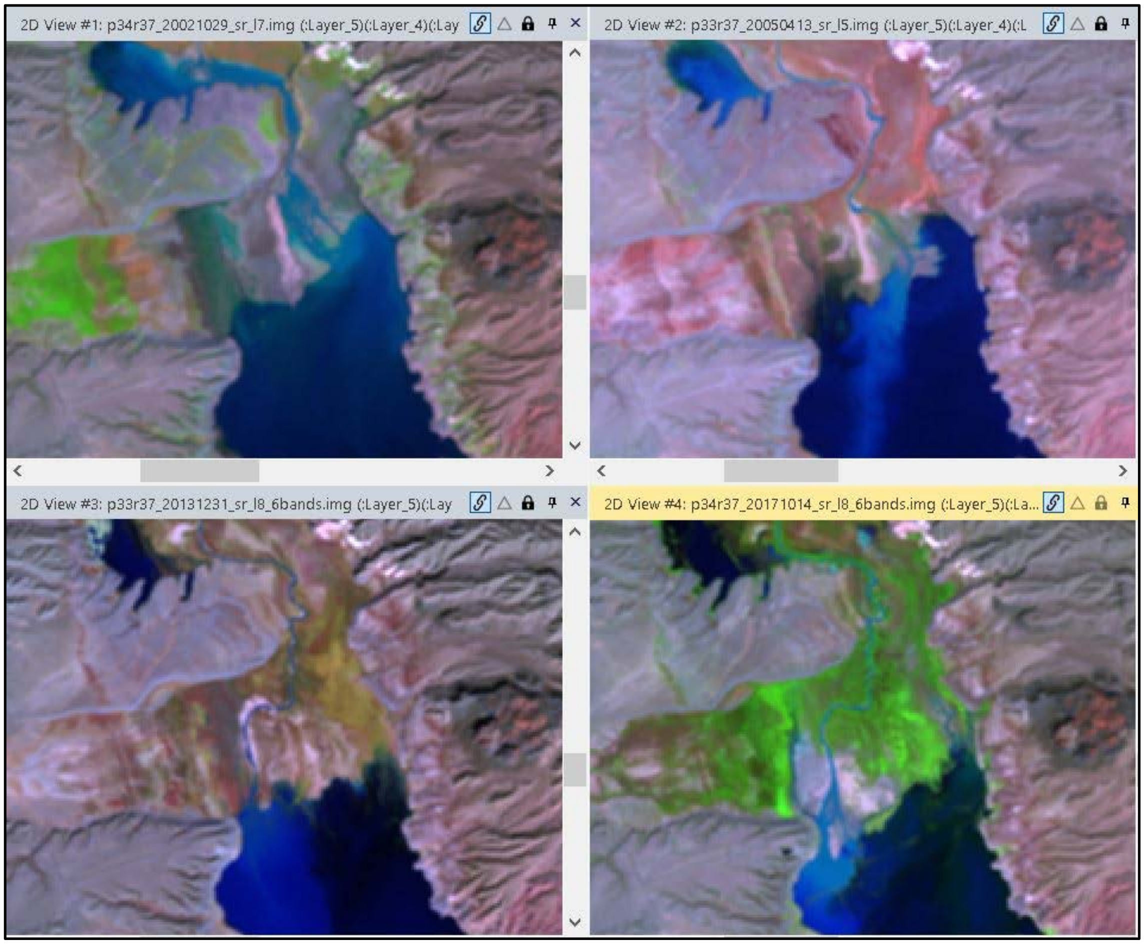

Figure 39. Rio Grande River inflow to Elephant Butte Reservoir at reservoir elevation ≈ 4320.9 feet.
Upper Left: 10/29/2002 (elev = 4320.90'), Upper Right: 4/13/2005 (elev = 4320.90'),
Lower Left: 12/31/2013 (elev = 4320.75'), Lower Right: 10/14/2017 (elev = 4320.88')

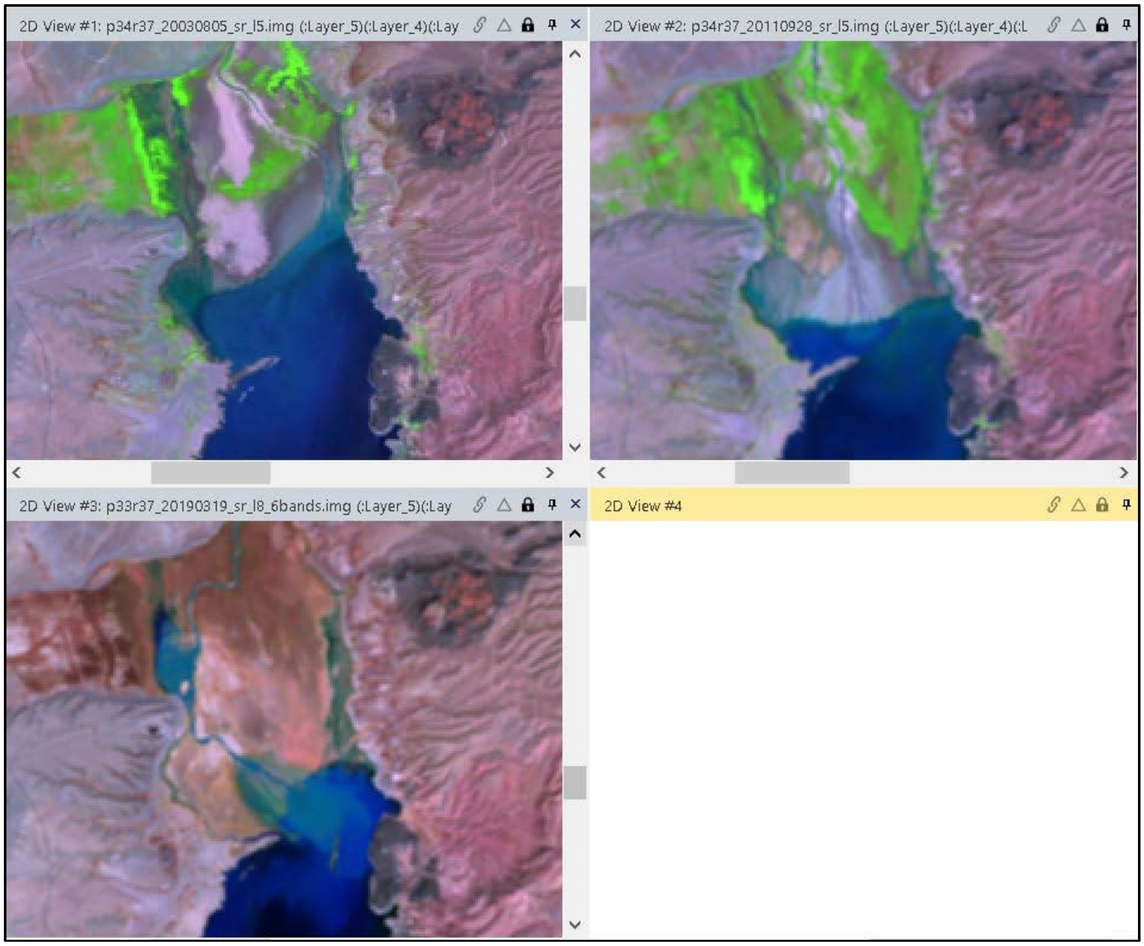

Figure 40. Rio Grande River inflow to Elephant Butte Reservoir at reservoir elevation ≈ 4311.6 feet.
Upper Left: 8/05/2003 (elev = 4311.5′), Upper Right: 9/28/2011 (elev = 4311.59′),
Lower Left: 3/19/2019 (elev = 4311.61′)

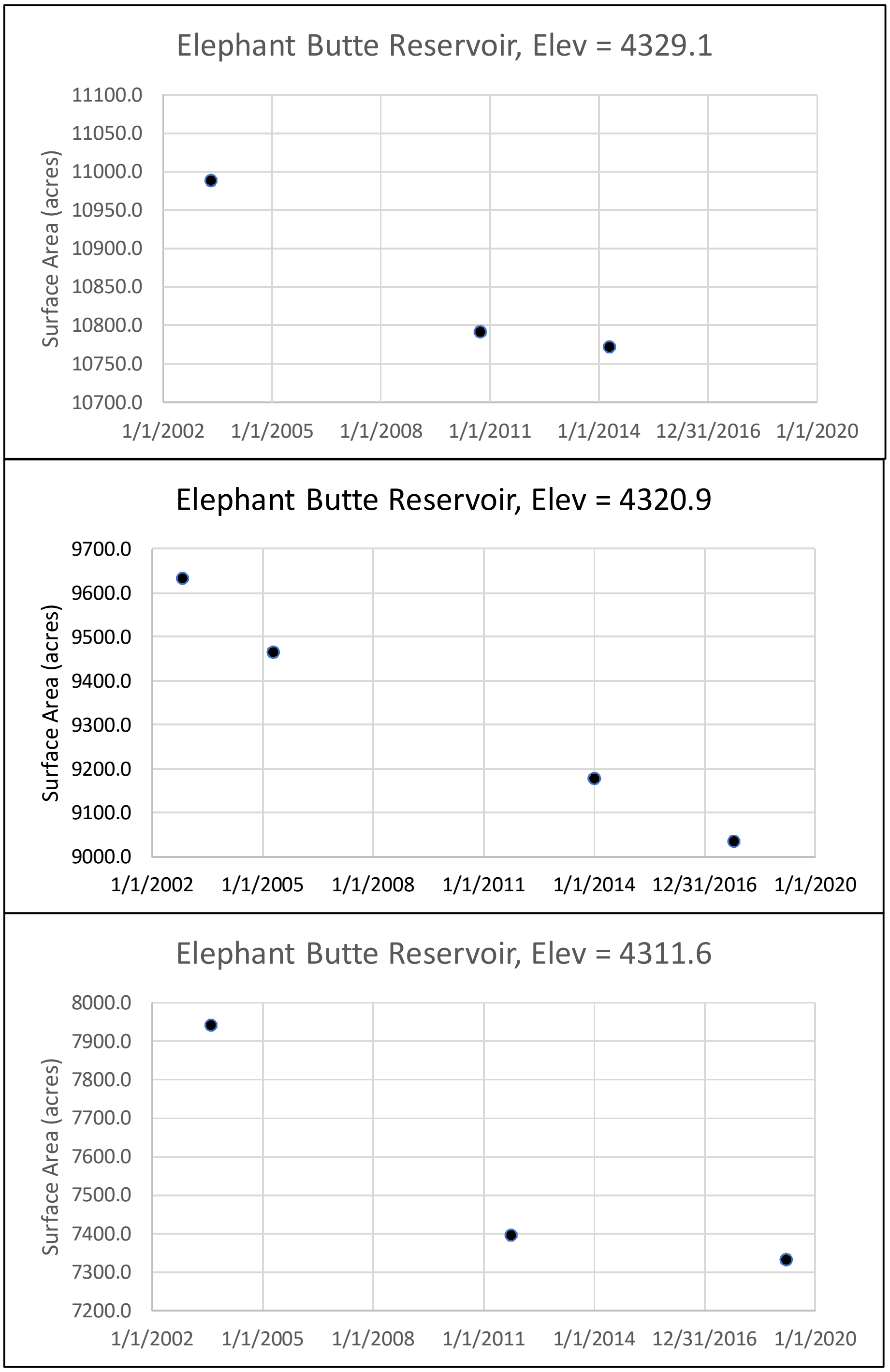

Figure 41. Changes in Elephant Butte Reservoir surface area over time at three different reservoir elevations.